Spectro-Photometric Analysis of Galaxy Merger Remnants with Tidal Features

by

Ophelie Karishma Leste

A THESIS SUBMITTED IN PARTIAL FULFILMENT OF
THE REQUIREMENTS FOR THE DEGREE OF

BACHELOR OF SCIENCE

in

Honours Astrophysics

(Department of Astronomy and Physics, Dr. Ivana Damjanov supervising faculty)

.....
.....
.....
.....
.....

SAINT MARY'S UNIVERSITY

May 31, 2021

Abstract

Spectro-Photometric Analysis of Galaxy Merger Remnants with Tidal Features

by *Ophelie Karishma Leste*

submitted on May 31, 2021:

We use 21 208 galaxies at redshifts $0.05 < z < 0.45$ with images from the Hyper Suprime-Cam Subaru Strategic Program (HSC-SSP) and accompanying spectroscopic observations from the Sloan Digital Sky Survey (SDSS) to study the properties of systems that host features of past mergers: streams and shells. We detect 251 shells and 774 streams through visual classification of the original and filtered galaxy images. We retrieve measurements of stellar mass and stellar population age for 16 936 galaxies from our sample. Galaxies with shells are more massive and older than both featureless galaxies and stream hosts, suggesting that they may be a result of major mergers. We analyse the star formation rates (SFR) for 6738 of our galaxies, derived from reliable measurements of $H\alpha$ available from the SDSS Legacy Survey. Shell hosts are predominantly among quiescent galaxies while stream hosts span the full range of SFR measurements. We construct diagnostic diagrams for 6778 galaxies to separate star forming galaxies from those that are dominated by Active Galactic Nuclei (AGN). A fraction (10%) of galaxies with streams show evidence of strong AGN activity, which may be a result of material being funnelled into the central region of

the host galaxy. In contrast, almost no shell hosts show the presence of strong nuclear activity. We measure the local density in the vicinity of our tidal feature hosts using data from the New York University Value-Added Galaxy Catalog (NYU-VAGC). We find that galaxies with features are, as expected, neither in isolated regions nor in clusters since these environments suppress mergers. We also observe that galaxies with shells tend to be in regions with slightly higher densities than the general population of galaxies. Based on sheer numbers and the distribution of the basic properties of the galaxies, we find that streams can occur in a vast range of galaxy mergers, while the formation of shells needs specific sets of conditions.

Contents

List of Figures

List of Tables

Chapter 1

Introduction

In modern cosmology, large galaxies are built up by star formation or via successive merging of smaller progenitors. Often time, those merger events leave behind unique morphological features in the galaxies' extended stellar halos, such as tidal streams, stellar shells, rings or plumes (Pop et al., 2017). This thesis focuses on the two main types of features described as streams and shells and their relation to the physical properties of their hosts.

1.1 Merger Signature

1.1.1 Streams

Stream-like structures are those that stretch along the hosts' orbits and sometimes wrap around the hosts multiple times (refer to second column of Figure 1.1.). The formation of streams is well understood. They are caused when individual stars are heated up by tidal forces from the host and leave the smaller companion galaxy through Lagrange points[1]. Depending on whether the stars are nearer to an inner (L_1) or outer (L_2 or L_3) Lagrange point (refer to Figure 1.2), the stream either stretches out into a leading trail or lags behind (Hendel et al., 2015).

[1]Lagrange points are positions in a system of bodies whose gravitational field interact, where the effective potential is at its maximum.

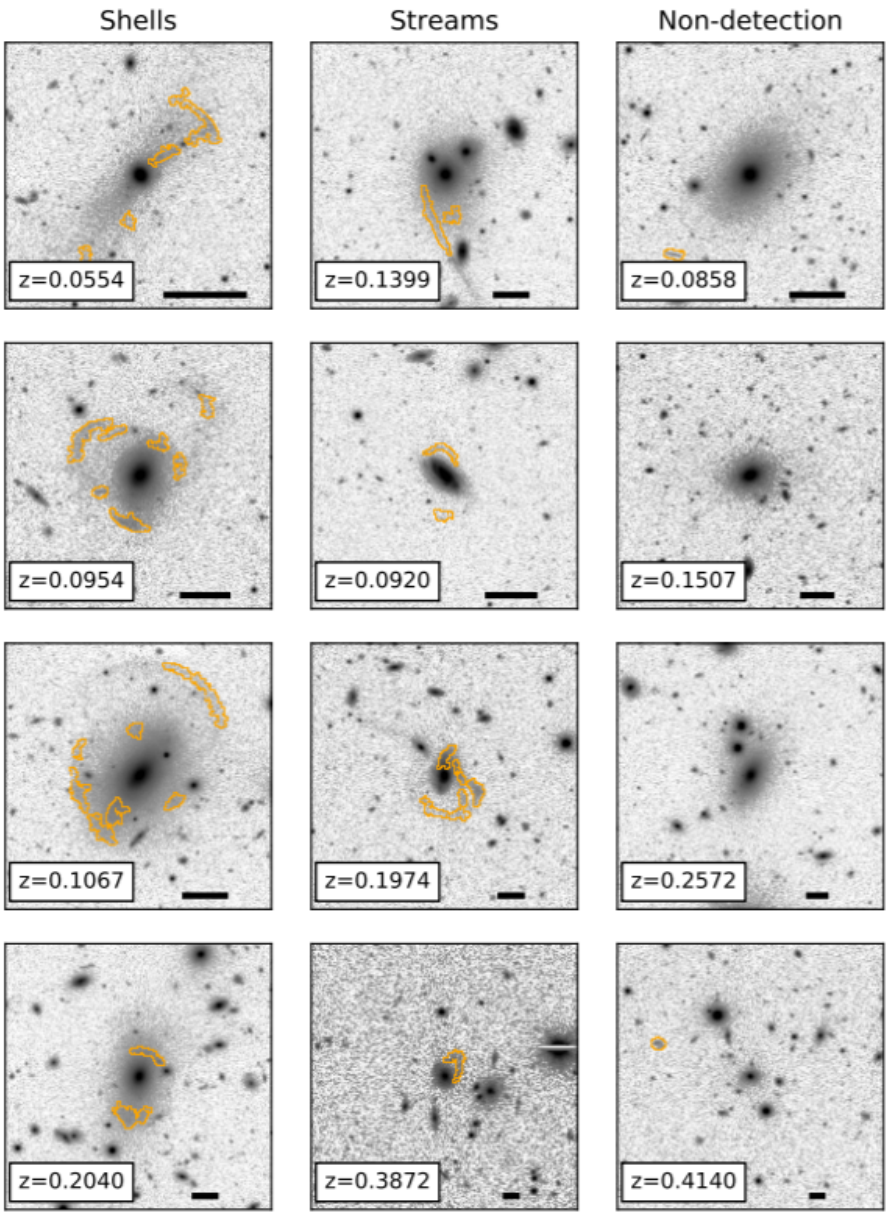

Figure 1.1: Features classified by Kado-Fong et al. (2018) showing geometrical appearance of shells (left column), streams (middle column) and featureless galaxies (right column) detected by their algorithm.

1.1.2 SHELLS

Structures defined as shells are those that form umbrella-shaped distribution of stars, extended significantly from the hosts, with their radius of curvature pointing towards

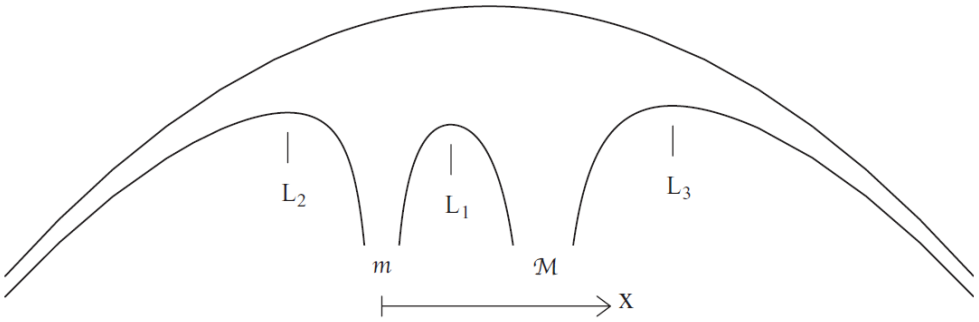

Figure 1.2: Diagram shows positions of Lagrange points, L_1 (inner), L_2 (outer) and L_3 (outer), with respect to two interacting bodies. Source: Sparke et al. (2007)

the center of the galaxies (first column of Figure 1.1). Previous theories have proposed that shells originate either from shock waves in the interstellar medium due to star formation or Active Galactic Nuclei (AGN) activity, or from density waves caused by passing galaxies (Fabian et al., 1980; Williams and Christiansen, 1985). However, observational studies are in favour of the merger scenario (Pop et al., 2017).

Most studies mainly considered minor mergers where one of the galaxies is significantly smaller than the other. However major mergers between galaxies of similar masses have also proven to produce shells. Mergers between massive satellites are more likely to produce shells than mergers between small satellites. The latter need more specific orbital parameters to result in shells. This is because the gravitational drag[2] is more important in major mergers than in minor mergers (Pop et al., 2017).

[2]gravitational drag, also known as the Chandrasekar friction, is the loss of momentum and kinetic energy of moving bodies through gravitational interactions with the surrounding matter in space.

1.2 Internal Properties of Galaxies with Tidal Features

Theoretical models of galaxy mergers predict that the internal properties of galaxies are dependent on the merging features that they host (Johnston et al., 2001). In this work, we use spectro-photometric datasets from the Hyper Suprime-Cam Subaru Strategic Program (HSC-SSP) and the Sloan Digital Sky Survey (SDSS) to explore how the presence of features is related to the following galaxy properties: the stellar mass, the stellar population age and the star formation rates.

1.2.1 Stellar Mass and Stellar Population Age

Spectral Energy Distribution

The measurements for the stellar mass and stellar population age are determined by fitting the spectral energy distribution (SED) of the galaxies. The different physical processes taking place in galaxies leave evidence on the shape of the spectrum, each dominating at different wavelengths. SED fitting methods work by fitting models to observed SEDs of galaxies in order to derive several physical properties simultaneously. Figure 1.3 shows an overview of the method used.

To construct the model SEDs, a number of elements need to be taken into account. The methods used to build the model spectra consider the evolution of the SED for a single stellar population with a single metallicity and abundance. The model then requires inputs such as the stellar evolution theory, the spectrum and the initial mass

function[3] (IMF). These components are combined into a time-dependent expression (Conroy, 2013). Models for different ages corrected for other variables, such as dust, are compared to the observed SED of the galaxy and the best fit model provides the stellar population age.

However, at this point the scale for the two SEDs differ as the model only considered a stellar population of 1 solar mass. Therefore, the best fit scaling factor for the two SEDs to match provides the stellar mass of the galaxy (Schneider, 2015).

D4000 Index

Another method to determine the age of a galaxy, is from the D4000 Index. D4000 is defined as the ratio of the average flux density after, to the one before the break at 4000 Å of the spectrum (Bruzual A., 1983). The discontinuity at 4000 Å is caused by the addition of several absorption lines in a small wavelength range, producing a thin opaque region, observed as a break in the spectrum.

D4000 strength can be used as an age indicator for the stellar population of galaxies as it is affected by the evolutionary stage of the constituent stars[4]. For instance, young hot stars contribute a large amount of flux below the 4000 Å break, therefore making the value of the ratio smaller. This, therefore indicates that the galaxy contains young stars which have short lifespans, meaning that the galaxy is younger.

[3]The IMF is the empirical function that describes the initial distribution of masses for a stellar population.

[4]Stars of different ages show absorption lines from different elements, contributing to different part of the spectrum

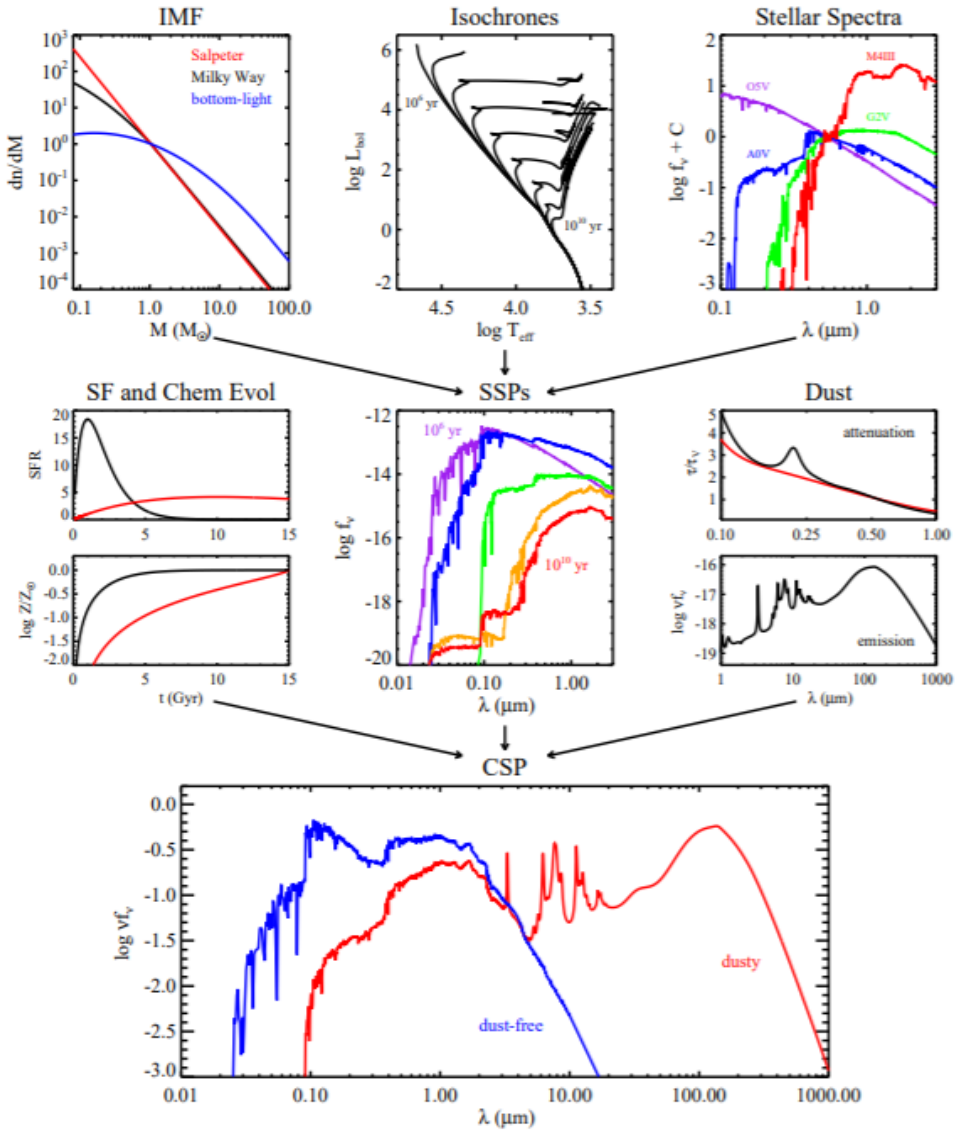

Figure 1.3: Steps in building up the SED: the top row shows the variables to construct a simple stellar population. The middle row shows how to construct a composite stellar population. The bottom row shows how the composite stellar population is corrected for dust and composition evolution. Source: Conroy (2013)

1.2.2 STAR FORMATION RATE

Studying emission line measurements of galaxies allows us to calculate their star formation rates (SFR). The SFR is the total mass of stars formed per year and it

describes how vigorously a galaxy is forming stars. It is often given in terms of solar mass per year or in terms of its specific star formation rate (sSFR), which is the SFR per unit stellar mass. Galaxies with low sSFR ($\log(sSFR) < 10^{-11}$ yr^{-1}) are called quiescent galaxies, while galaxies with larger $\log(sSFR)$ values are described as star forming galaxies(Whitaker et al., 2017).

Integrated light measurements in the ultraviolet (UV), far-infrared (FIR), or nebular recombination lines, provide information on the star formation properties of galaxies. In our case, we used $H\alpha$ emission lines, which provide a direct evidence to the presence of young massive stellar population (Kennicutt, 1998). Around young hot stars, $H\alpha$ photons are produced by interstellar gas ionised by high energy radiations from the stars. Therefore measuring the strength of $H\alpha$ emission is proportional to the current amount of young hot stars present in the galaxy.

1.2.3 IONISATION MECHANISM IN NEBULAR GAS

As seen in the previous section, ionised interstellar material in galaxies produces a number of emission lines. The ratios of the strength of these lines provide clues for the processes that are responsible for the ionisation in the nebular gas. Particularly in this thesis, we consider low ionisation species such as [OIII], [NII] and [SII], with respect to $H\alpha$ or $H\beta$ (Kewley et al., 2006).

These line ratios allow us to distinguish between HII region-like objects (those that are dominated by star formation) or galaxies that are dominated by AGN activity. Emission lines due to AGN activity come from the interaction of the radiation

from the central black hole with the surrounding accreting material (La Mura et al., 2017). AGNs are separated into Seyferts, which are high-ionisation AGNs containing optically thick accretion disks and LINERs (Low Ionisation Narrow Emission-Line Regions) which are low-ionisation AGNs with optically thin accretion disks (Véron-Cetty et al., 2000). LINERs are more common, however the cause of their AGN power source is still being debated.

Diagnostic diagrams, named after "Baldwin, Phillips Telervich" (BPT Diagrams, Baldwin et al., 1981), are used to visualise the relationship between the different line ratios and separate the different types of galaxies. As shown in Figure 1.4(a), galaxies that are predominantly star forming are found at positions of low values of [NII]/$H\alpha$ and high values of [OIII]/$H\beta$ to positions of high [NII]/$H\alpha$ and low [OIII]/$H\beta$ in BPT Diagrams. The AGN region starts at the end of the star forming region and extends towards high [OIII]/$H\beta$ and [NII]/$H\alpha$. Composite galaxies are those whose spectra are dominated by both star formation and AGNs (Kewley et al., 2006). They are found between the HII region and the AGN region on the BPT diagram.

1.3 External Properties

Several previous studies have shown that galaxies are influenced by their environments (Tinker and Conroy, 2009; Ellison et al., 2009; Kang et al., 2017). In Section 1.2, we describe how different tidal features are related to the merger history of their hosts. As galaxy interactions are also dependent on the environment in which they happen, we intend to connect the external properties of the host galaxies to their tidal features.

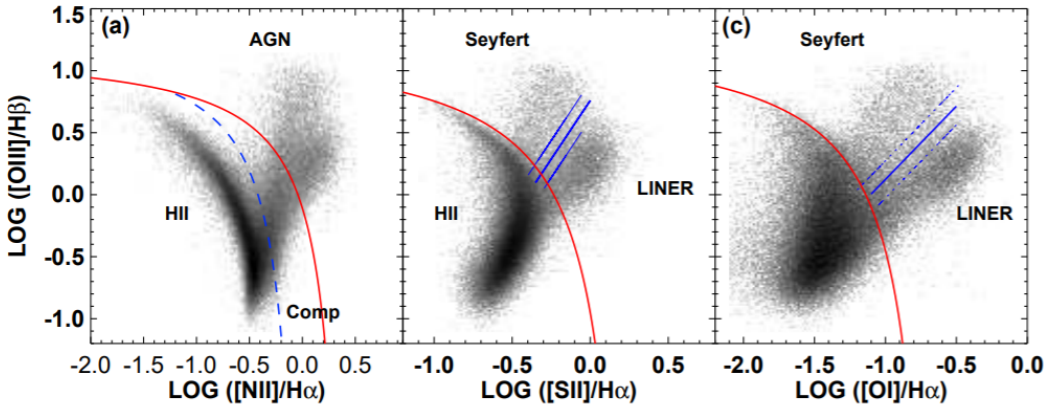

Figure 1.4: Example of a BPT diagram from Kewley et al. (2006) showing the position of the different types of galaxies with respect to their emission line ratios. Red line in (a) shows the separation between star forming galaxies and AGNs.

The environment of a galaxy is described by how other galaxies are distributed in its vicinity. Galaxies can be isolated, that is, they do not have any major companions but may have a few small satellites. They can also be found in small or large groups (clusters), where they are surrounded by other galaxies of fairly similar masses. Elliptical galaxies, which are the most common type of galaxies in the local universe, are more likely to be found in high density environments, while spiral galaxies are preferentially found in low density environments.

To study galaxy environments, two categories of methods are used: those considering a specified number of nearest neighbours to find the underlying density fields and those that find the number of galaxies in a fixed aperture around the target galaxy (Muldrew et al., 2012). The first method is independent on the dark matter halo mass, while the aperture-based method identifies the high density region corresponding to high mass haloes.

We speculate that if a certain tidal feature host is found to be predominantly

isolated, it would most likely signify that this type of remnant (with either shells or streams) was formed from a single merger in the history of the host and that it may be the only merger the galaxy experienced. On the other hand, if a tidal feature is most likely to be found in clusters, it would suggest that the feature is a result of frequent interaction between the host and its environment.

1.4 Motivation

The idea that the interactions between galaxies generate tidal features is well-established. However, the frequency of occurrence of different remnants (shells or streams) is not fully understood. Tidal features have low surface brightness (LSB) and thus are more likely to be found in deep imaging surveys. They are related to galaxy mergers that are not very common and thus large area (volume) surveys are required to find them. In recent years, large-area deep imaging surveys have been producing large data volumes allowing astronomers to create large statistical samples of galaxies with tidal features. The combination of these imaging surveys with similar large spectroscopic surveys provides the information on how the presence of tidal features is related to the history of mass assembly of their host galaxies.

1.5 GOALS

In this study we examine spectro-photometric measurements to probe properties of galaxies hosting shells, streams and those with no apparent features, following up

the work of Kado-Fong et al. (2018). Our aim is to find the relationships between the merger remnant features and the internal properties of the hosts, such as stellar mass, stellar population age and star formation rate. We explore how the features may be changing the aspects of the host galaxies. We also determine whether the mergers leading to the formation of the features affected the activity in the center of the galaxy and speculate if one is dependent on the other. We further inspect the environment of the galaxies to find the relationships between the occurrence of the features and their neighbourhood.

Throughout this work we adopt cosmology of $\Omega_m = 0.3$, $\Omega_\Lambda = 0.7$ and $H_0 = 70$ kms^{-1}Mpc^{-1}, except for instances where the New York University Value-Added Galaxy Catalog is used, where $H_0 = 100$ kms^{-1}Mpc^{-1}.

1.6 STRUCTURE

We describe the survey and sample selection, as well as the method to reclassify the tidal feature hosts in Chapter 2. In Chapter 3 we study the trends in the basic properties of the different feature host galaxies, such as the stellar mass, stellar population age and their star formation rates. In Chapter 4 we use emission line measurements to construct diagnostic diagrams and separate the dominating ionising mechanisms in galaxies with features. We determine the local densities around galaxies harbouring shells and streams in Chapter 5 to determine whether they are found preferentially in specific types of environments. We conclude in Section 6.

Chapter 2

Data Set

2.1 Parent Sample

The full dataset of galaxies have spectra from SDSS Data Release 12 (DR12, Alam et al., 2015), therefore have known spectroscopic redshifts in a range of $0.05 < z < 0.45$. We use stellar mass and stellar population age derived from Maraston et al. (2009), which fits stellar evolution models to the SDSS photometry using SED fitting methods described in Section 1.2.1. The age listed is defined as the time elapsed from the start of the star formation period using a model with an exponentially declining star formation rate. We obtain emission line kinematics results for our sample from Maraston et al. (2011) and Thomas et al. (2011).

The sample includes galaxies from both the SDSS Legacy Catalog (complete to $r < 17.77$ mag, Strauss et al., 2002), and the Baryon Oscillation Spectroscopic Survey of SDSS-III (BOSS, roughly complete from stellar mass, Dawson et al., 2002). The sample is dominated by galaxies from the latter. Measurements for star formation rates and D4000 index are available for objects in the SDSS Legacy Catalog, derived in the manner described in Brinchmann et al. (2004). The number of galaxies available from the different datasets are given in Table 2.1.

Table 2.1: Number of galaxies in different datasets

Survey/Dataset	Number of Galaxies
BOSS (Dawson et al., 2002)	14123
SDSS Legacy Catalog (Strauss et al., 2002)	6738
Measurement from SED fitting (Maraston et al., 2009)	16936

2.2 SDSS Galaxies with Tidal Features

The full sample of 21 208 galaxies was first classified by Kado-Fong et al. (2018). They used an algorithm that detects any low surface brightness features in images from HSC-SSP. This wide-field survey is conducted on the 8.2 m Subaru Telescope, covering the Wide layer of 1400 deg^2 in five broad bands (grizy) and the Deep layer of 26 deg^2 in four fields (Aihara et al., 2018). The telescope has a wide field of view, which allows us to cover large area of the sky and to explore galaxies in a vast range of environments. Due to the high sensitivity of the camera, we are able to probe faint objects and also faint (low surface brightness) regions around bright galaxies, which is essential for the scope of this thesis.

Kado-Fong et al. (2018) performed their classification by detecting high spatial frequency components out of convolved images of the galaxies. The images had their central light source masked for better visibility of possible features (Figure 2.1). These detections are then classified visually into shells and stream hosts.

2.2.1 Reclassification

After examining the classification by Kado-Fong et al. (2018), by comparing the images before and after the filtering, we noticed some obvious misclassifications. For

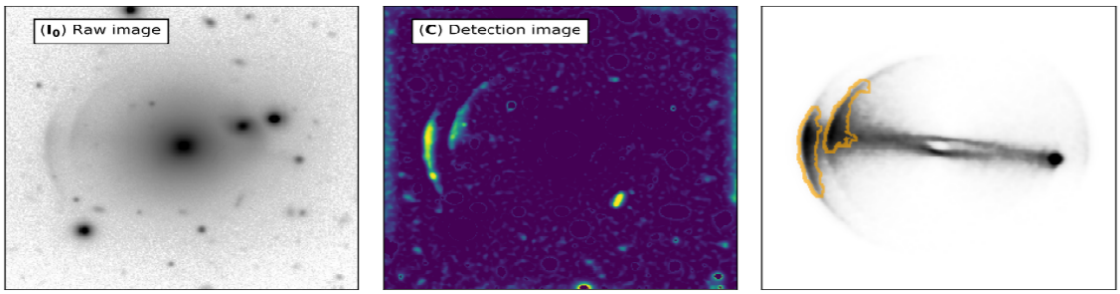

Figure 2.1: Simulation of detection of shell hosts by Kado-Fong et al. (2018). Image on the left shows image (normalised and background-subtracted image) before the filtering. The middle image is the convolved image. The rightward image shows the outline of the detected feature, which is then visually classified as shells.

Table 2.2: Classification of features

Classifier	Shells	Streams
Kado-Fong et al. (2018)	214	987
Our classification	251	774

instance, some artefacts that appear as features in the filtered image in fact do not belong to the central galaxy(Figure 2.2). This is important for our analysis, since we are studying properties of galaxies that host these features. Another example of misclassification is that spiral arms can appear as merger galaxy remnant features in the filtered image. In Figure 2.3, we see an example where Kado-Fong et al. (2018) classified the galaxy as a stream hosts by only viewing the filtered image (right panel). However, when comparing with its unfiltered image, we see that the structure appearing in the filtered image is not an extended feature, as streams are defined, but is within the galaxy's disk and can actually be a part of its spiral arms.

We decided to reclassify the whole sample. The images are filtered in a similar fashion to the method of Kado-Fong et al. (2018). All the images are classified visually, considering both the raw image and the filtered image to minimise misclassifications

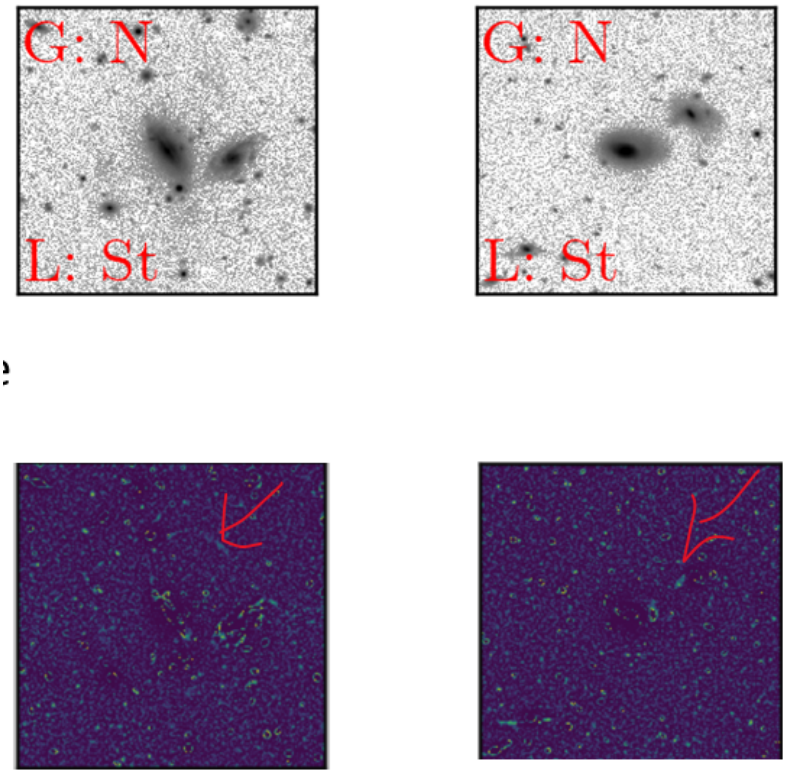

Figure 2.2: The four panels show two unfiltered images (top) and their corresponding convolved images (bottom) of streams detected by the literature. Artefacts appearing as features in the filtered image are found to not be features when compared to the unfiltered image. Instead, these features belong either to neighbouring galaxies (left column) or to undisturbed (regular) structure of the host galaxy (right column).

(Figure 2.4). We find 1025 feature hosts while Kado-Fong et al. (2018) found 1201, as shown in Table 2.2. Both classifications agree for 239 streams and 58 shells. We use this new improved classification for further inspection of the galaxy properties.

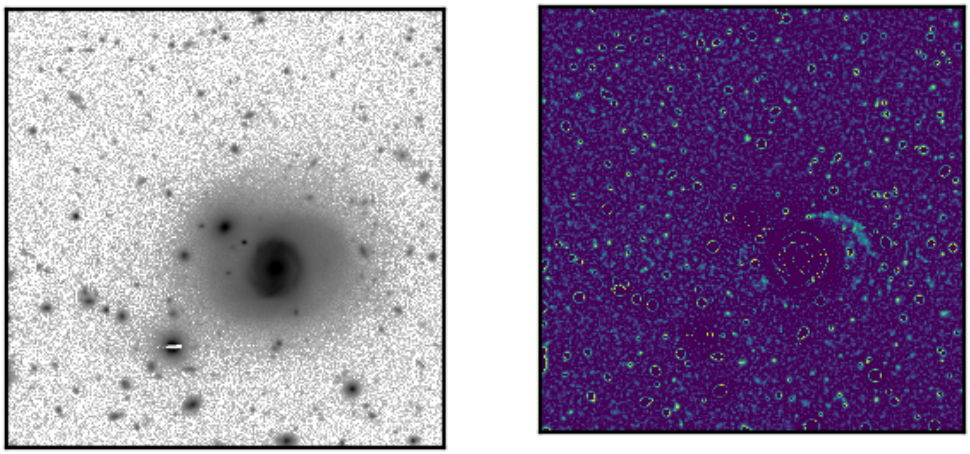

Figure 2.3: Left panel shows the unfiltered image classified as having streams by Kado-Fong et al. (2018), but when comparing both the filtered and unfiltered image, we see that the artefacts appearing as streams in the filtered image (right) are within the galaxy disk, and in fact not an extended feature, and may actually be the spiral arms of the galaxy.

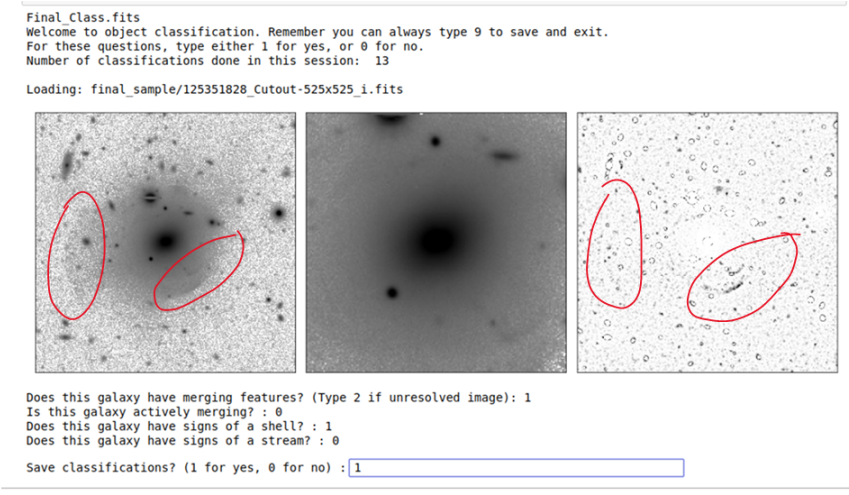

Figure 2.4: Example of the workflow for viewing and classifying the galaxies prepared by Harrison Souchereau. Shell features are shown circled in red. In this case the features are more visible in the original image (left) than in the filtered image (right). This galaxy was classified as a shell host both by us and Kado-Fong et al. (2018).

Chapter 3

Basic Properties of Host Galaxies

We examine the basic properties of stream and shell host galaxies relative to galaxies with no detected features. There are a number of fundamental properties that are shaped by the way the galaxies assembled their mass. In the following sections we look at the stellar mass, the stellar population age and the star formation rates of the galaxies harbouring tidal features.

3.1 Stellar Mass

Maraston et al. (2009) derived stellar mass from SED fitting, as described in Section 1.2.1. They used two models of spectra: the passive model, which is based on the superposition of two single-burst models with identical age and metallicity with the age as the only parameter, and the star forming model which has an exponentially declining star formation rate with the age defined as the time elapsed from the beginning of the star formation. Maraston et al. (2009) advise that for galaxies with colour $(g-i) < 2.35$, the star forming model should be used. The majority of galaxies in our sample are bluer, with colour $(g-i) < 2.35$ (16936 galaxies, 80% of the parent sample), thus it is sensible to only consider measurements using the star formation model for our analysis.

In Figure 3.1, we compare the stellar mass distribution of galaxies with features (stream and shell hosts separately) and non-interacting galaxies. Galaxies without features have $\log(M_*/\mathrm{M}_\odot)$ ranging from 8.5 to 12. Masses for stream hosts spread throughout the whole range, while the masses for galaxies with shells only cover the range from the 10^{th} to the 95^{th} percentile of the distribution of featureless galaxies.

The left panel in Figure 3.1 shows the normalised frequency distribution of the galaxies' stellar mass. The normalisation is computed by dividing the frequency in each bin by the maximum frequency. The right panel of the figure shows the cumulative distribution which is found by summing the frequency of each consecutive bin and then normalised in the same way as the histogram[1].

By inspecting the stellar mass histograms in Figure 3.1 visually, we find that the distribution for galaxies with streams does not differ from that of galaxies without features. On the other hand, 95% of the galaxies with shells have stellar masses above $10^{10} M_\odot$. We performed Kolmogorov–Smirnov test (KS test, Karson, 1968) to decide if the mass distributions of host and non-interacting galaxies differ from each other. Results from the KS test return the p-value, which tells us whether or not to reject the null hypothesis that two independent samples come from the same distribution. If the p-value is high (by convention > 0.05), we cannot reject the hypothesis that the distributions of the two samples are the same. The results from comparing the distributions for galaxies with streams and those without features produce a high p-value, thus tells us that we cannot reject the null hypothesis and suggests that the

[1] all frequency/cumulative frequency histograms presented here are constructed in the same manner

two distributions are similar. When comparing the distribution between galaxies with shells and those without features, we obtain a p-value much below 1% and we can reject the null hypothesis.

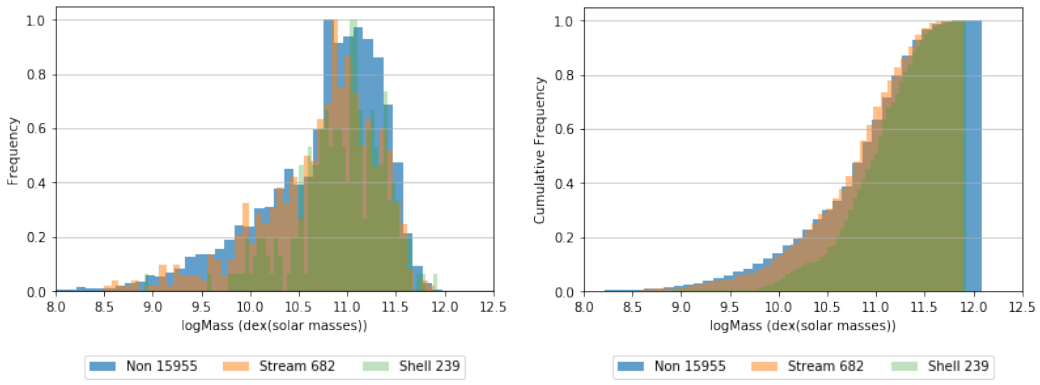

Figure 3.1: Distribution of stellar mass measurement from SED fitting (Maraston et al., 2009). Population labelled "non" represent galaxies with non-detections of features. The left panel shows the normalised histogram and on the right, the normalised cumulative distribution. Distribution for shell hosts tends towards higher masses. KS test confirms that there is no evidence of difference between the distribution of stream hosts and featureless galaxies.

3.2 Stellar Population Age

The measurements for the stellar population age (which tells us the age of the stars that contribute the most to the light of the galaxy) are derived from SED fitting (Section 1.2.1). We select the measurements from Maraston et al. (2009) as described in Section 3.1, using the derivations from SED fitting with the star forming model, where the age is defined as the time elapsed from the start of the star formation period.

We compare the distributions of the stellar population age for galaxies with and

without features in Figure 3.2. In the left panel of the figure, showing the normalised distribution of our galaxies' age, we see that half of the general population of galaxies in our sample have ages ranging from 1 Gyr to 3 Gyr and that the highest age measured is 12 Gyr. In the cumulative frequency distribution shown on the right panel of Figure 3.2, it appears that galaxies with streams tend to be younger than both featureless galaxies and those with shells. Results from KS test comparing the distribution for galaxies with and without streams, produce a p-value well below 1%, confirming that the two distributions differ from each other. It also visually appears that galaxies with shells have older ages, but this observation cannot be confirmed with enough confidence from statistical tests.

We also look at the distribution of D4000 index available for galaxies in the SDSS Legacy Survey (Brinchmann et al., 2004), as a measure of the mean age of their stellar population. D4000 index is a direct spectroscopic measurement from the galaxy's spectra, unlike the age measurement mentioned above, which is a result of fitting models to the SED. If the SED fitting is done correctly, measurements for age and the D4000 index should reflect similar results.

The distributions comparing D4000 measurements for the tidal feature hosts and the underlying population of galaxies (Figure 3.3), give clearer insights on the trends followed by shell hosts, than does the distribution of age derived from SED fitting. As described in Section 1.2.1, a large D4000 index indicates an old stellar population. Here we confirm that galaxies with shells tend to be overall older than the general population of galaxies and we can reject the null hypothesis that the distribution for galaxies with shells and without features are the same, with a p-value of 10^{-11} from

KS test results between the two samples.

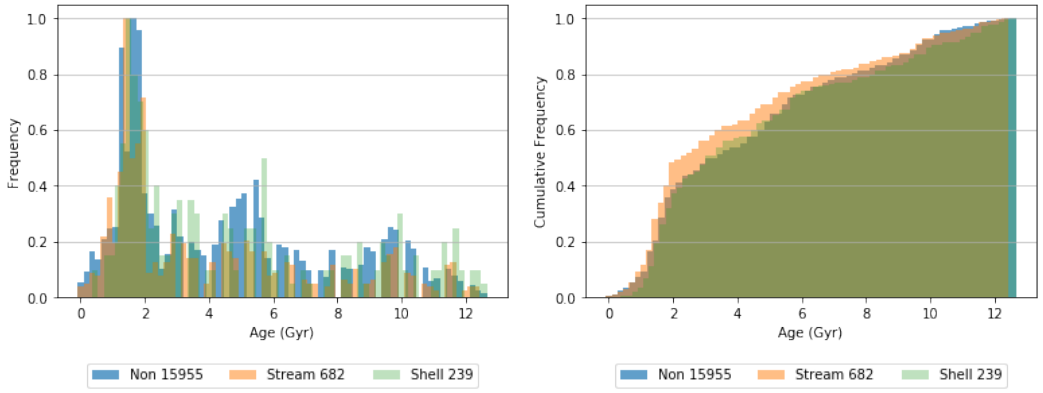

Figure 3.2: Distribution of stellar population age measurement from SED fitting (Maraston et al., 2009). Left panel shows the normalised frequency distribution and the right panel shows the normalised cumulative distribution. KS-test results show that distribution for stream hosts and galaxies without features are sampled from different populations.

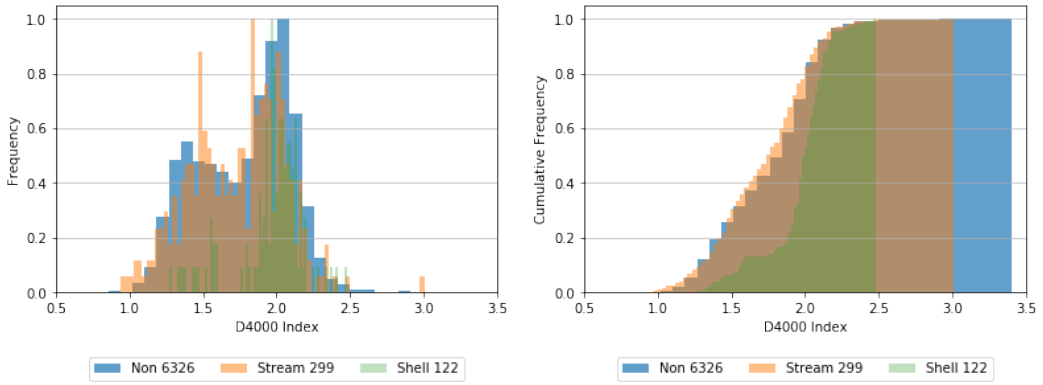

Figure 3.3: Distribution of D4000 measurement from Brinchmann et al. (2004), as a proxy for age. Left panel shows the normalised frequency distribution and the right panel shows the normalised cumulative distribution. The majority of shell hosts have larger D4000 values.

Figure 3.4 shows the relationship between the stellar mass and the age (in terms of the D4000 index) for galaxies in the SDSS Legacy Survey (Brinchmann et al., 2004). We see that less massive galaxies in the diagram tend to have lower D4000 values ($< 1.5 - 1.6$). In contrast, more massive galaxies ($\log(M_*/M_\odot) > 11$) have

higher D4000 indices, which is in agreement with observation made by Kauffmann et al. (2003). As shell hosts predominantly occupy the upper right region of the figure (where more massive galaxies are), they are therefore on average more massive and older than galaxies with streams. These observations adhere to the proposition made in Section 1.1.2, that galaxies with shells are more likely to be formed from major mergers, as those interactions would result in more significant growth in mass.

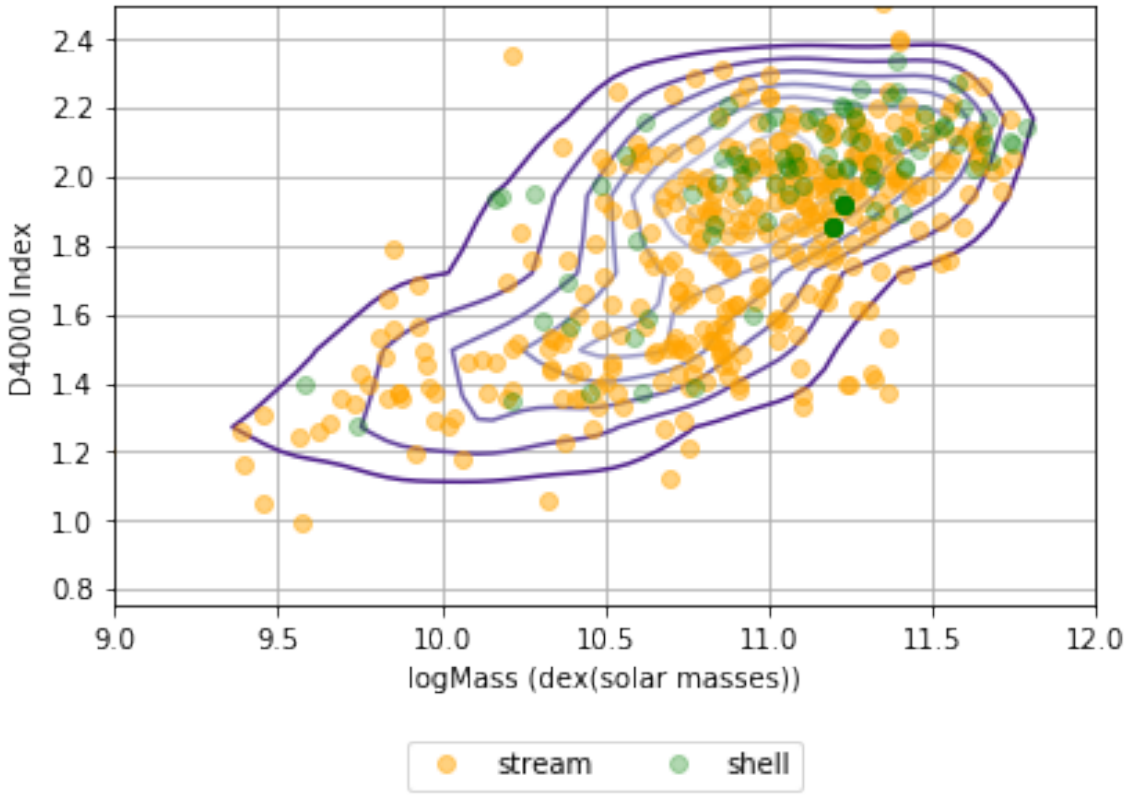

Figure 3.4: D4000-Mass diagram with contours showing the continuous probability density curve in 2-D of the population of featureless galaxies and the position of host galaxies. Shell hosts, on average, occupy positions of high mass and older age. Stream hosts are spread throughout the distribution.

3.3 Star Formation Rate

We selected measurement for SFR based on the strength of $H\alpha$ emission lines, available for objects in the SDSS Legacy survey (Brinchmann et al., 2004). In the right panel of Figure 3.5 we see that the distribution for the general population of galaxies have two peaks. The first at low SFR, around $10^{-1}M_*$/yr and the second at higher rates, around $10^{0.5}M_*$/yr, thus separating our sample in nearly two distinct categories: quiescent galaxies (with low SFR) and actively star forming galaxies.

By visually comparing the distributions of galaxies with streams or shells to those without features, we see from the histograms in Figure 3.5 that stream hosts have SFR covering the full range of the measured values. According to KS test results (p-value at 0.019), the distributions for galaxies with streams and those without features differ and from the cumulative histogram (Figure 3.5), stream hosts are slightly more star froming. We can also reject the null hypothesis that the distribution for shell hosts and featureless galaxies are the same as the p-value from KS test between the two distribution is far below 1%. We see that galaxies with shells tend to be more quiescent (85% of shells with $\log(SFR) < 0.0$). This observation is in agreement with results in Section 3.2, where galaxies with shells are older, as older galaxies are less likely to be forming stars.

Previous studies have found that there is a relationship between the star formation rate of galaxies and their assembled stellar mass (Noeske et al., 2007; Daddi et al., 2007; Elbaz et al., 2007). Star forming galaxies form a tight sequence between SFR and stellar mass, known as the galaxy 'main sequence' of star formation (Wuyts et al.,

2011), which implies that star formation for the majority of galaxies is powered by quasi-steady processes.

We analyse the position of the host galaxies in the log(SFR) versus stellar mass diagram (Figure 3.6). In the figure, we see the galaxy 'main sequence' for star forming galaxies ($SFR > 10^{0.5} M_*/yr$) , demonstrating that the relationship between the SFR and the stellar mass is directly proportional. Galaxies with shells are in the lower right region of the diagram, with low SFR and large masses. This again correlates with previous statements we made about shell hosts. It is expected that these galaxies are quenched, in relation to their higher mass and older age.

In comparison, galaxies with streams have SFR spread over all the regions covered by the underlying population (Figure 3.6), regardless of their stellar masses. Stream hosts are also more star forming than galaxies with shells, even at similar masses. We suppose that the streams can be funneling material into the host galaxy, causing the compression of the interstellar gas and thus triggering star formation.

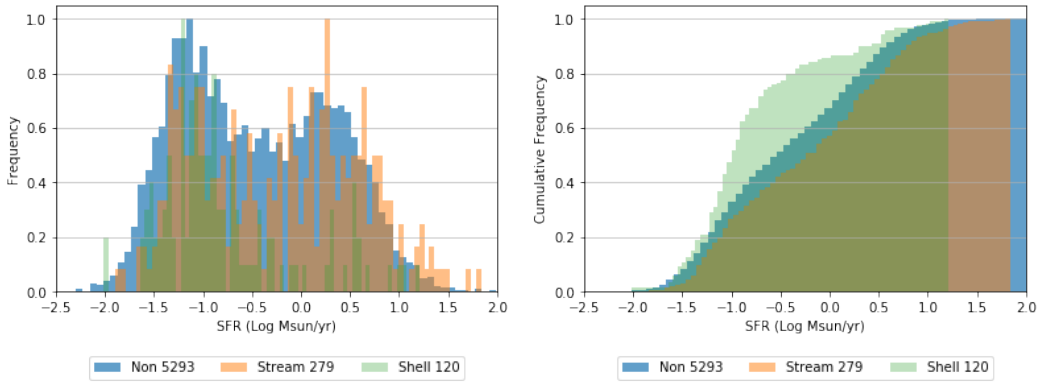

Figure 3.5: Distribution of log(SFR) for objects in SDSS legacy survey (Brinchmann et al., 2004). Left panel shows the normalised frequency distribution and the right panel shows the normalised cumulative distribution. Shell hosts have lower SFR. We can reject the null hypothesis that the distribution for stream hosts and featureless galaxies are the same from the KS test results.

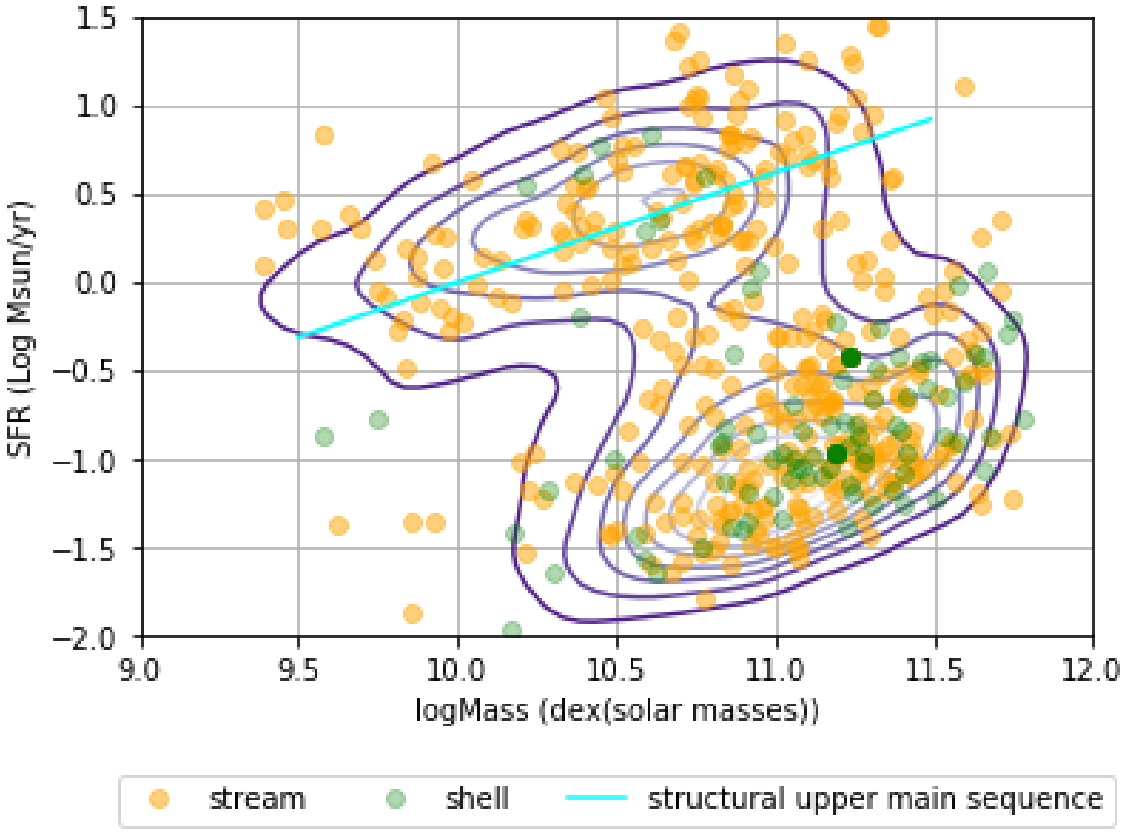

Figure 3.6: log(SFR) - log(Stellar Mass) diagram with contours showing the continuous probability density curve in 2-D of the population of featureless galaxies and the position of host galaxies. Upper main sequence (blue line) represents the Main Sequence relation of star forming galaxies. Majority of shell hosts are in the bottom right of the diagram, region of low SFR and high stellar mass. Streams are spread throughout the distribution.

We also look at the distribution of the stellar mass with respect to the specific star formation rate (sSFR), which is the SFR per unit stellar mass (Figure 3.7). As expected, we see that the relationship between sSFR and the stellar mass flattens and we recover the two distinct star forming and quiescent populations. Our conclusion that shell hosts are less star forming remains unchanged and we see that for a given stellar mass galaxies with streams are more star forming than those with shells.

In Figure 3.8 we look at the relationship between the age (in terms of D4000 Index)

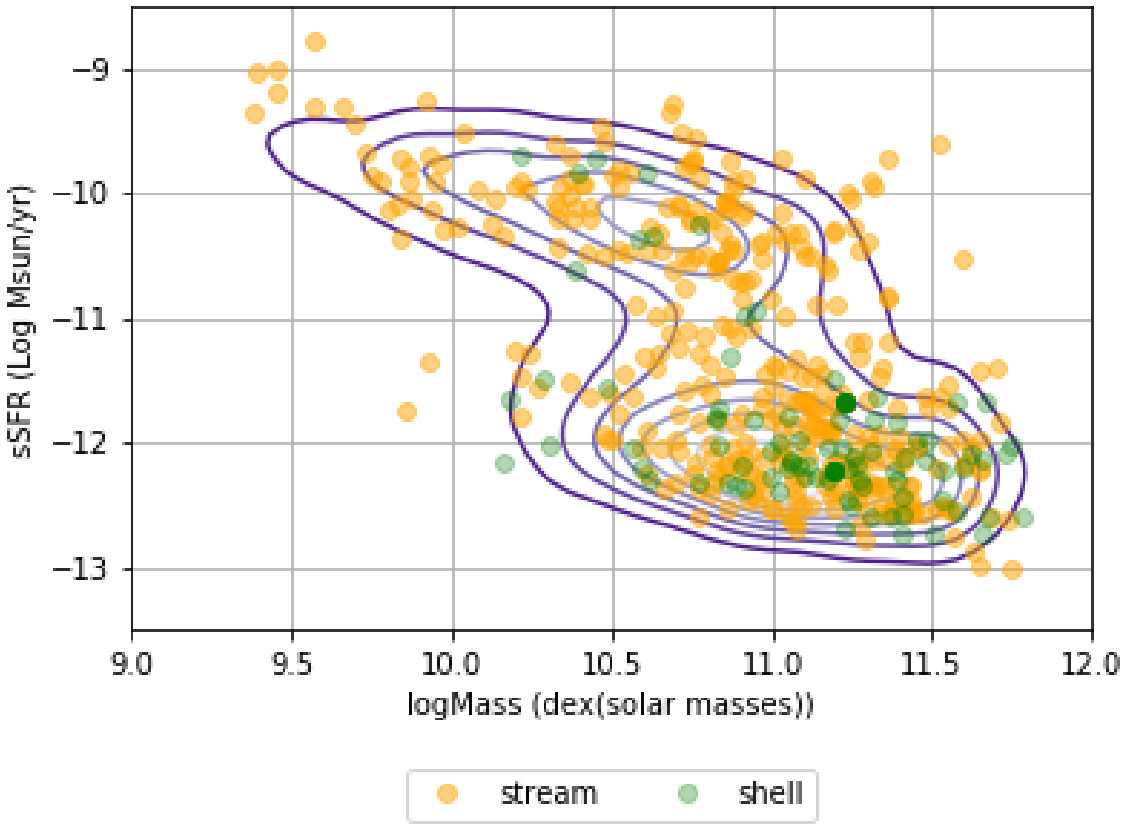

Figure 3.7: log(sSFR) - log(Stellar Mass) diagram with contours showing the continuous probability density curve in 2-D, of the population of featureless galaxies and the position of host galaxies. 80% of shell hosts have $\log(sSFR) < -11$ and $\log(M_*/M_\odot) > 10.5$.They are in the bottom right of the diagram, region of low SFR and high stellar mass. Streams are spread throughout the distribution.

and the star formation rates. We see the evolution tract of the general population of galaxies (purple contours) where the SFR decreases proportionally with age. The SFR for galaxies with streams follow the distribution of the general population of galaxies. On the other hand, 90% of shell hosts are found in the bottom right region of the plot, among the old and quiescent galaxies. This observation is in agreement with simulations made by Cooper et al. (2011), where it is possible for streams to evolve into shells as the host galaxy ages or to form later in the merger history of

their hosts.

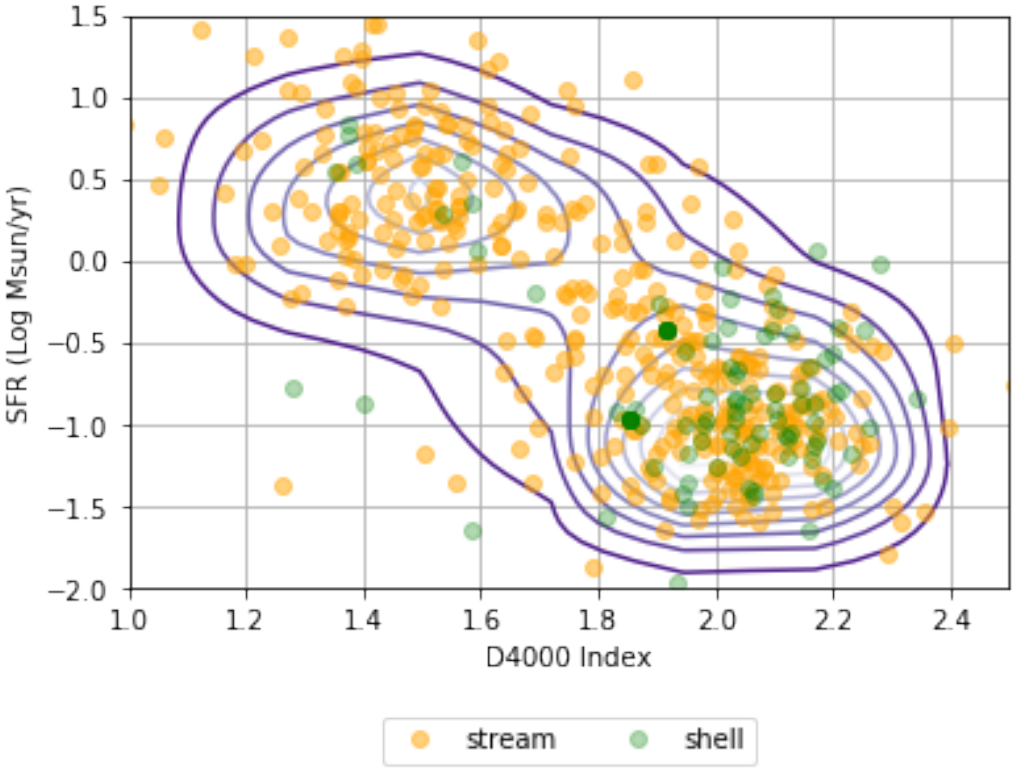

Figure 3.8: log(sSFR) - D4000 diagram with contours showing the continuous probability density curve in 2-D, of the population of featureless galaxies and the position of host galaxies. Shell hosts are in the bottom right of the diagram, region of low SFR and old stellar population age. Streams are spread throughout the distribution. We see the evolution tract of decreasing SFR as galaxies age.

3.3.1 SFR calculation from $H\alpha$ emission lines

The number of galaxies with measured SFR in the SDSS legacy survey (Brinchmann et al., 2004) is 5676, which is only 27% of the total sample. In an attempt to extend the sample measurement for SFR, we use emission line flux measurement of $H\alpha$ available from Maraston et al. (2011) and the method described by Kennicutt (1998) to calculate the star formation rate for galaxies in our sample:

$$SFR = log(10^{-41.28} L(H\alpha)), \tag{3.1}$$

where L($H\alpha$) is the emission line flux intensity of $H\alpha$.

We correct observed $H\alpha$ emission line flux for dust attenuation, following the equation from Kong et al. (2002),

$$\tau_v = \frac{-\ln[F(H\alpha)/F(H\beta)] - \ln[B]}{(\frac{\lambda(H\alpha)}{5500})^{-0.7} - (\frac{\lambda(H\beta)}{5500})^{-0.7}}, \tag{3.2}$$

$$I(H\alpha) = F(H\alpha) e^{\tau_v (\frac{\lambda(H\alpha)}{5500})^{-0.7}}, \tag{3.3}$$

where τ_v is the effective V-band optical depth, B is the Intrinsic Balmer Flux Ratio and is 2.87 for star forming galaxies, $F(H\alpha)$ and $F(H\beta)$ are the measured fluxes and $I(H\alpha)$ is the attenuation corrected flux of $H\alpha$. We obtain the dust corrected intrinsic luminosity in $H\alpha$, used in Equation 3.1 to find the SFR, from the flux calculated in Equation 3.3 using the flux-luminosity-distance equation:

$$L(H\alpha)) = I(H\alpha) * 4\pi D_L^2, \tag{3.4}$$

where D_L is the luminosity distance to the galaxy.

We find that it is necessary to have a Signal-to-Noise ratio $S/N > 3$ for all emission lines used. Taking into account the corrections necessary, we were unable to further extend the sample of SFR measurements using this method. However, we recover the same results as the measurements from the SDSS legacy survey (Brinchmann et al.,

2004).

Chapter 4

Ionisation of the Nebular Gas in Galaxies with Tidal Features

4.1 BPT Diagram of the Parent Sample

As described in Section 1.2.3, we use the classification lines described in Kewley et al. (2006) to separate the different ionisation mechanisms in the nebular gas of galaxies in our sample (Figure 4.1). The maximum starburst line (Ke01, Kewley et al., 2001):

$$\log([OIII]/H\beta) = 0.61/(\log([NII]/H\alpha)0.05) + 1.3, \tag{4.1}$$

is the upper bound to the star forming sequence. That is, galaxies found below the line in the diagram have ionisation mechanisms dominated by star formation.

Those star forming galaxies are further divided into pure star forming galaxies and composite galaxies, whose spectra have significant contribution from both AGN and star formation (Ka03, Kauffmann et al., 2003):

$$0.61/(\log([NII]/H\alpha)0.05) + 1.3 = \log([OIII]/H\beta). \tag{4.2}$$

We further classify galaxies that have their emission lines dominated by AGN activity (that is galaxies which are found above the maximum starburst line Ke01,

Table 4.1: Number of galaxies in different BPT Classifications for full sample from Maraston et al. (2011) and the corresponding number of galaxies with streams or shells in each BPT classes.

BPT	All Galaxies	Shell Hosts	Stream Hosts
Composite	1959	21	111
LINER	1735	38	104
Seyfert	441	3	33
Star Forming	2642	17	115

Eq. 4.1), into LINERs and Seyferts (Section 1.2.3). This is done by comparing their ratios of $[SII]/H\alpha$ and $[OIII]/H\beta$ as follows:

LINERs−

$$\log([OIII]/H\beta) < 1.89\log([SII]/H\alpha) + 0.76, \tag{4.3}$$

Seyferts−

$$\log([OIII]/H\beta) > 1.89\log([SII]/H\alpha) + 0.76. \tag{4.4}$$

We select emission line measurements available for our sample from Maraston et al. (2011) with $S/N > 3$, resulting in a sample of 6778 galaxies. Galaxies below Ka03 (Eq. 4.2) are purely star forming. Those found between the Ke01 (Eq. 4.1) and Ka03 (Eq. 4.2) lines are classified as composite galaxies and the ones above the Ke01 (Eq. 4.1) line are dominated by AGNs. The latter are further classified as Seyferts or LINERs according to Equations 4.4 and 4.3. The summary of our BPT diagnostics for galaxies in our parent sample with available emission lines is given in Table 4.1 and their position in the BPT diagram is shown in Figure 4.1.

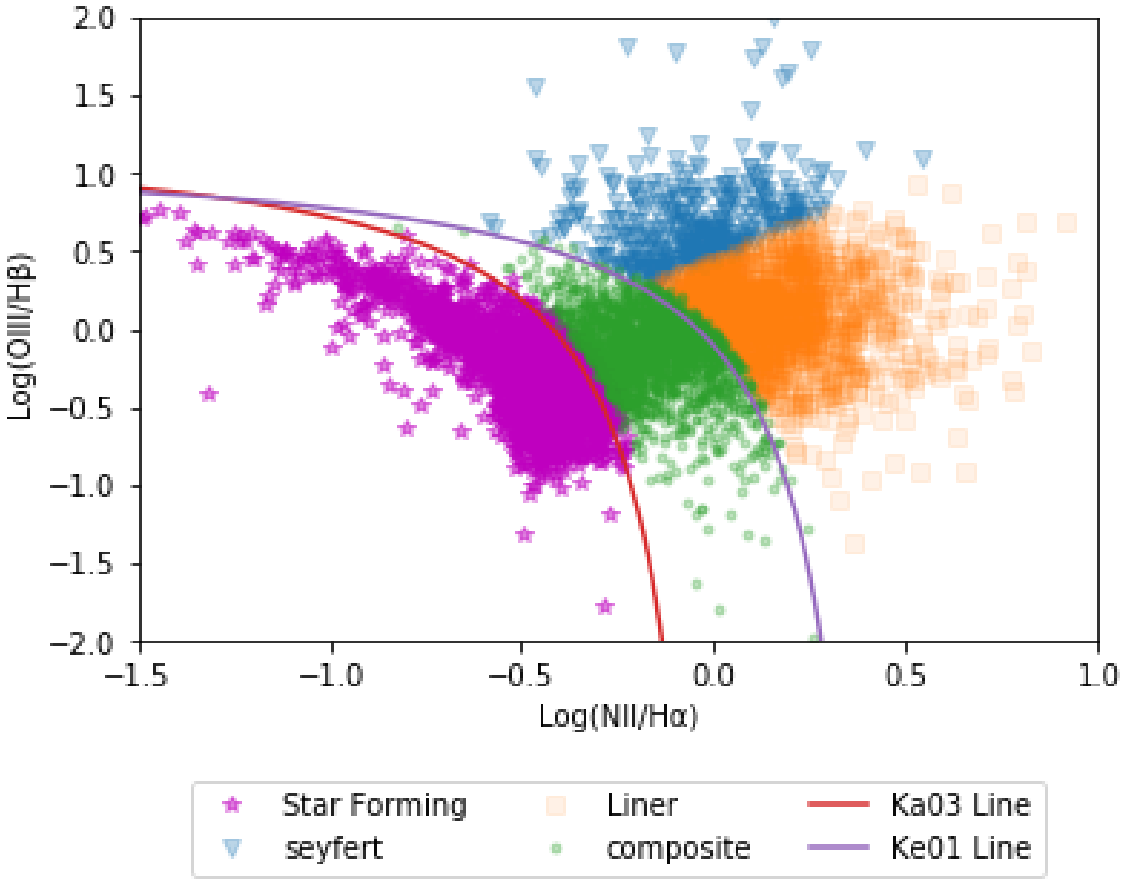

Figure 4.1: BPT diagram for the sample of 6778 galaxies from parent sample with available emission line measurements from Maraston et al. (2011). Galaxies in the different BPT classes are shown in different colours. The plot shows Ke01 (eq. 4.1, purple line) and Ka03 (eq. 4.2, red line).

4.2 Frequency of Different Ionisation Sources in Galaxies with Tidal Features

To have a better understanding of the correlation between the merger remnant features and the ionisation processes, we look at the distribution of the features throughout the BPT classification (Figure 4.2). Here it appears that the highest fraction of galaxies with streams are star forming and that a higher percentage of shell hosts have signs of AGN activity (classified as composite or LINER) than the general population

of galaxies.

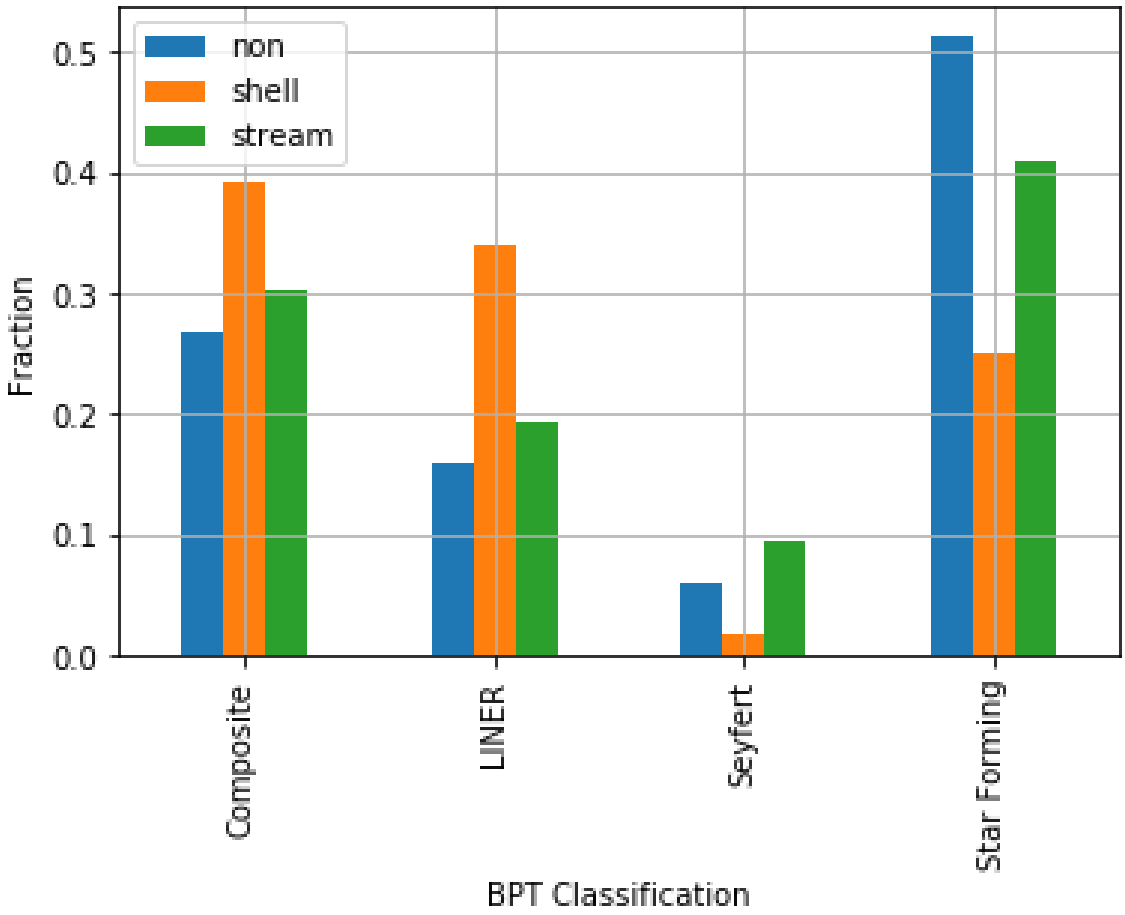

Figure 4.2: Distribution comparing BPT classification of shell and stream hosts to featureless galaxies. There is a significant amount of shell hosts with AGNs (composite or LINER) compared to stream hosts. Stream hosts are predominantly star forming.

Because the stellar mass of galaxies is an important determinant of galactic properties (Section 3.1), we sampled the population of galaxies without features according to the mass distribution of the each feature host to make a more direct comparison for the BPT distribution. We select featureless galaxies that have stellar mass distributions equal to that of galaxies with features (streams or shells).

The left panel of Figure 4.3 is an example which shows that the mass distribution

of shell hosts and the subsample of featureless galaxies are the same. The right panel shows how the two samples with matched mass distributions from the left panel are distributed in the BPT diagram.

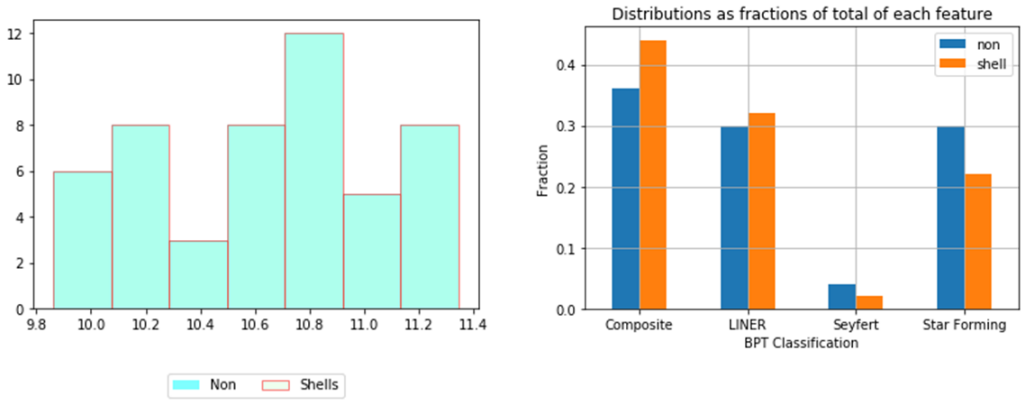

Figure 4.3: On the left, the diagram shows one example of matching of the mass distribution between shell hosts and featureless galaxies. On the right is the BPT classification for this resulting sample of shell hosts and featureless galaxies.

We then create 1000 of such subsamples of galaxies without tidal features that follow the mass distribution of feature (either shell or stream) hosts. For each of these created subsamples, we reconstruct the BPT distribution as in Figure 4.3. We then summarise our findings by averaging the fractions of galaxies with different gas (ISM) ionisation mechanisms from all 1000 subsamples.

In Figure 4.4 we compare the resulting distributions of the BPT-based classification of shell and stream hosts with respect to the population of galaxies of similar mass. The fractions are calculated from the number of galaxies in each bin divided

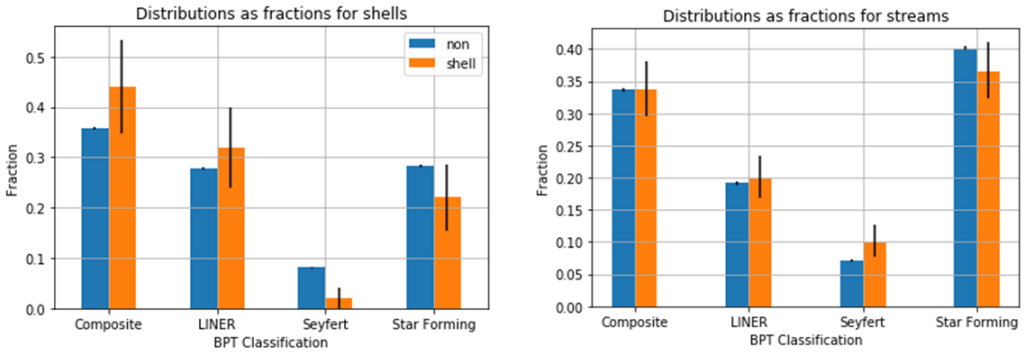

Figure 4.4: Comparison of BPT-based classification for galaxies that host shells (left) and streams (right) and their mass-matched counterpart galaxies without features.

by the total number of galaxies in each respective samples (total shell hosts, stream hosts and non-detections separately). The errors E_n on the galaxies without features are computed from Poisson Statistics:

$$E_n = \frac{\sigma_c}{\sqrt{1000}}, \tag{4.5}$$

where σ_c is the standard deviation of the normal distribution of the fraction in a bin (left panel of Figure 4.3) for all 1000 iterations.

The asymmetric errors on the feature hosts are:

$$upper = \frac{\sqrt{N_c + 3/4} + 1}{N_f}, \tag{4.6}$$

$$lower = \frac{-\sqrt{N_c + 1/4}}{N_f}, \tag{4.7}$$

where N_c is the number of galaxies in a bin and N_f is the total number of shells or streams (Gehrels, 1986). This representation of errors alongside our results is necessary as the frequencies are determined from small numbers of observed events (galaxies with shells and streams in each BPT classes). The confidence limits (upper and lower) need to be presented for proper comparison between the BPT classes of galaxies with and without tidal features.

From the results in the left panel of Figure 4.4 the most statistically significant difference between shell hosts and featureless galaxies is that the ionisation mechanisms are substantially less dominated by Seyfert AGNs for galaxies with shells, while the other processes seem to be equally distributed (within error bars). Seyfert galaxies have quasar-like nuclei, that is, they are very luminous in the visible light spectrum and have active supermassive blackholes at their centers. Thus, our observations suggests that the centers of shell hosts are less active than the general population of galaxies of similar mass.

Comparing the distribution of stream hosts and the population of galaxies without features, in the right panel of Figure 4.4, we see again that the more compelling difference is in the fraction of Seyfert galaxies. However in this case, there is a higher percentage of Seyfert AGNs among stream hosts than among featureless galaxies with similar masses. This relates to previous suggestions that streams are funnelling material into the host galaxy (Section 3.3), but this time the material goes towards

the central accreting (super)massive blackhole.

From the contour maps shown in Figures 4.5 and 4.7 we see the correlation between the dominating ionisation mechanisms and the basic properties of the galaxies with shells. As expected, we observe that galaxies with AGN activity are more massive and older (panels showing LINERs, Seyferts and Composites in Figure 4.5). This is consistent with the tendency of AGNs to reside in more massive hosts, which correlates to older galaxies as described in Section 3.2. Galaxies with dominant AGN activity (LINERs and Seyferts in Figure 4.7) also tend to have low star formation rates, which is in agreement with previous studies exploring the scenario where AGN feedback quenches star formation (negative AGN feedback) and promotes the evolution of young blue galaxies into red galaxies (Vitale et al., 2013). The fact that emission line galaxies with shells are predominantly ($> 75\%$ of shell hosts) either composite galaxies or LINERS, further reinforces the idea that the formation of shells requires a major merger involving the generation of ionising shock waves from AGN feedback.

On the other hand, by comparing the contour maps for galaxies with streams (Figure 4.6), we see that the stream hosts have a larger spread in ages altogether than the galaxies with shells (as seen in Section 3.2). Comparing Figures 4.7 and 4.8, we see that stream hosts are more star forming overall than shell hosts. This again follows the proposition that there are processes supporting star formation in galaxies with streams. We also see that 30% of stream hosts among the composite galaxies are star forming. Another scenario for galaxies with streams besides the direct effect of triggered star formation by the infall of material in the disk region of the galaxy, is that the stream in composite galaxies is fuelling the accretion disk

around the central black hole and result in positive AGN feedback (unlike the case with shell hosts above) causing the compression the interstellar gas and igniting star formation (Zubovas et al., 2017).

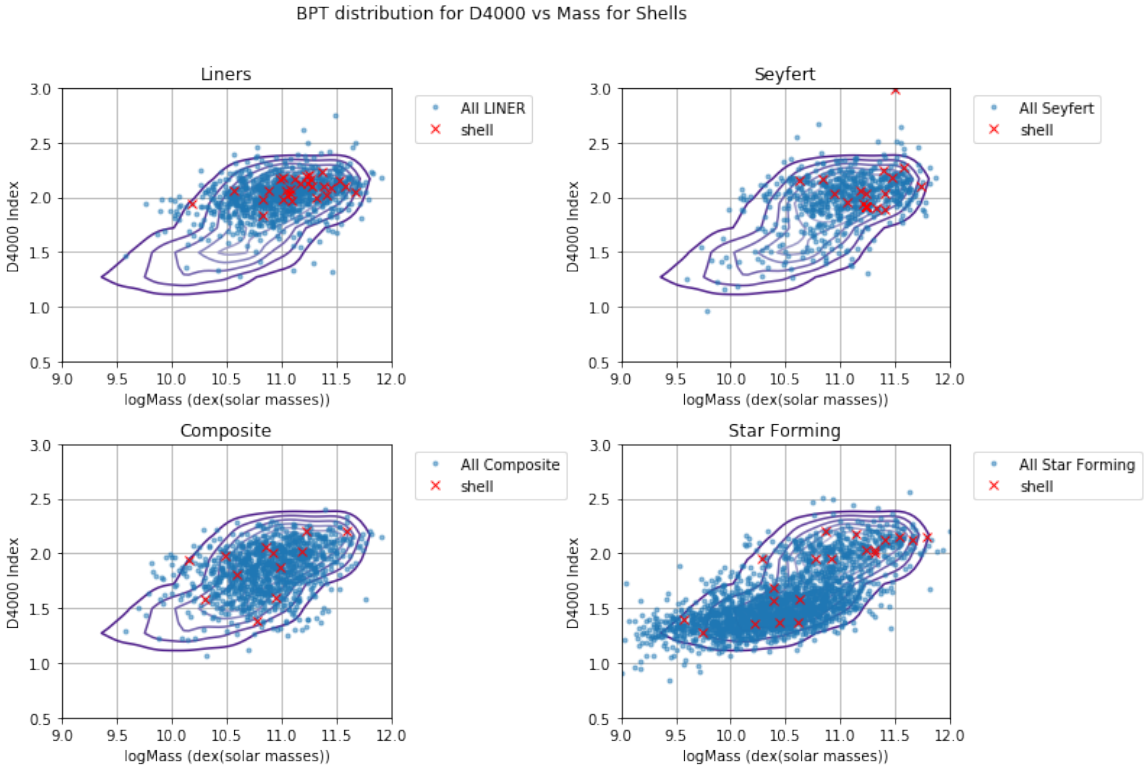

Figure 4.5: D4000-Stellar Mass diagram with contours showing the continuous probability density curve in 2-D of the population of featureless galaxies and the position of shell hosts. Each panel shows the position of galaxies belonging to separate BPT-based classification. The blue points shows the population of all galaxies classified as either LINERs, Seyfert, composite or star forming. The red cross shows the position of shells in each of the BPT classes.

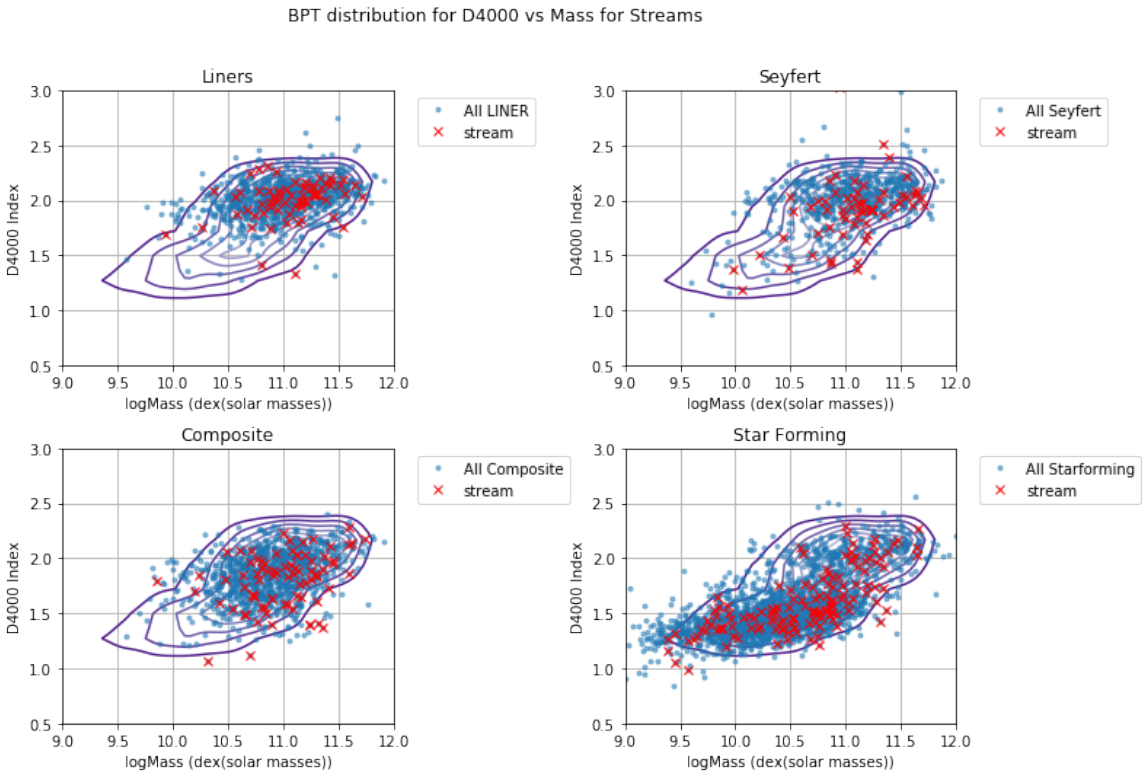

Figure 4.6: Same as for Figure 4.5, but for galaxies with streams.

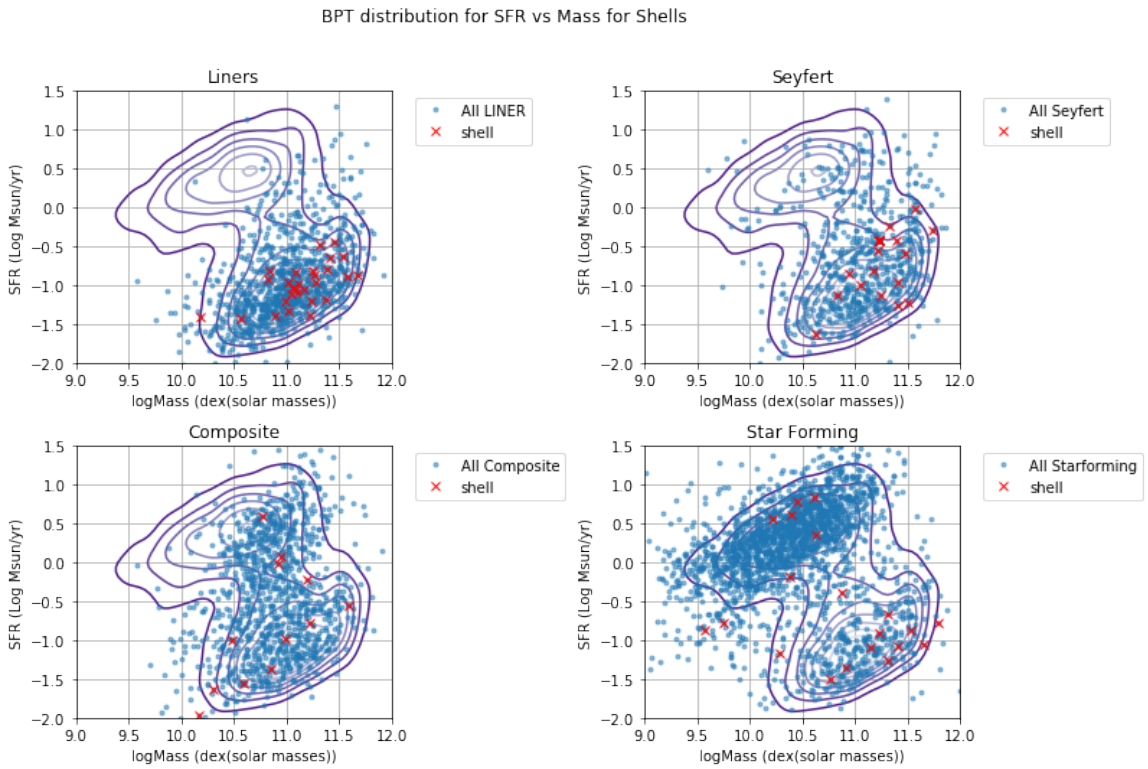

Figure 4.7: SFR-Stellar Mass diagram with contours showing the continuous probability density curve in 2-D of the population of featureless galaxies and the position of shell hosts. Each panel shows the position of galaxies belonging to separate BPT-based classification. The blue points shows the population of all galaxies classified as either LINERs, Seyfert, composite or star forming. The red cross shows the position of shells in each of the BPT classes.

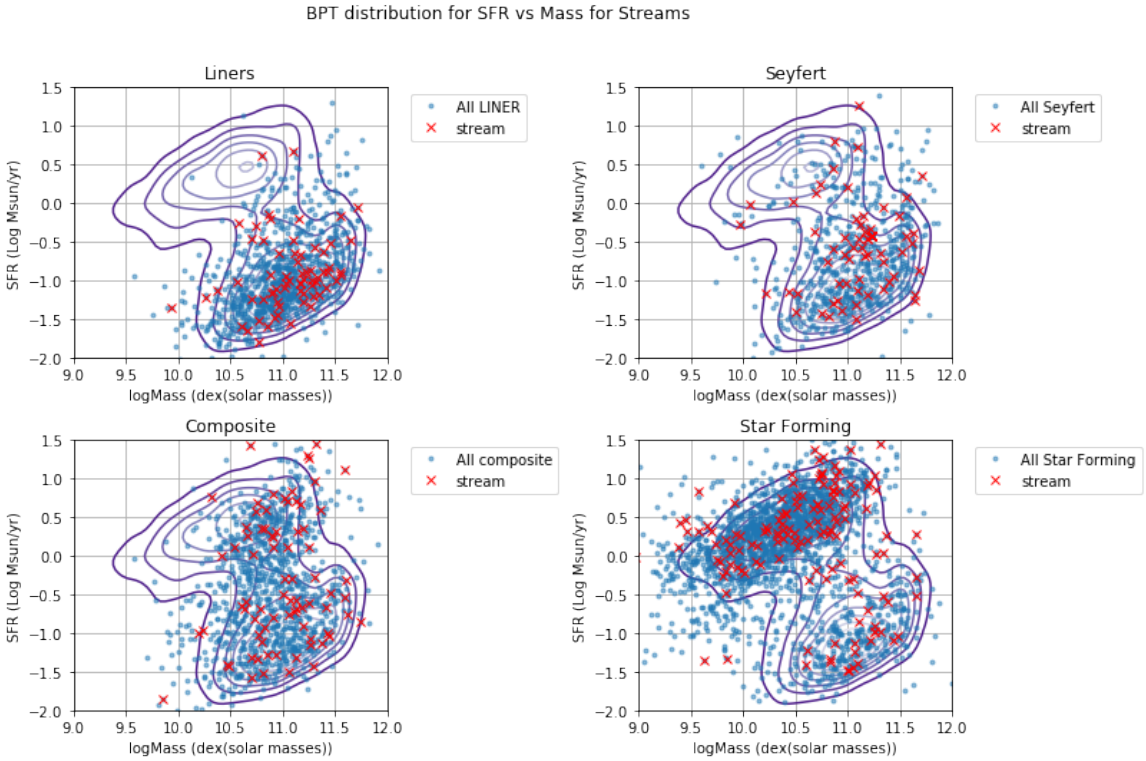

Figure 4.8: Same as Figure 4.7, but fro galaxies with streams.

Chapter 5

Environment of Galaxies with Tidal Features

5.1 Measuring Environment

As mentioned in Section 1.3, there are two ways to describe the environment of a galaxy: it can either be defined in terms of the distance to a fixed n^{th} nearest neighbour, or in terms of the number of galaxies in a fixed aperture around a target galaxy. In this thesis we consider the underlying density field as a function of the distance to the fifth nearest neighbour, r_{5NN}.

The nearest neighbour method is more accurate for probing the 'local environment' of a galaxy, that is the region within a single dark matter halo (Muldrew et al., 2012). The value of the n^{th} neighbour we select is important as the method loses in effectiveness if n is larger than the number of galaxies in the halo. We study the local environment rather than the large scale structure as we seek to know the galaxy densities that favour interaction.

5.1.1 Data Set for Measuring Environment

We use the New York University Value-Added Galaxy Catalog (NYU-VAGC), which is a catalog of galaxies at redshifts $z < 0.3$ based on the SDSS Data Release 2 (DR2).

Table 5.1: Number of galaxies from NYU-VAGC and feature hosts in the different regions described in Figure 5.1.

Region	NYU-VAGC	Feature Hosts
A	4326	97
B	2867	83
C	4203	294
D	1677	29

The sample contains 343 568 objects in 7966 deg^2 of spectroscopic coverage and have redshift determinations with approximately 85% completeness. The catalog contains all information necessary for statistical studies of galaxy properties and their large scale structure derived from photometric and spectroscopic measurement of galaxies, such as K-corrections and structural parameters. The NYU-VAGC is described in detail in Blanton et al. (2005).

In this thesis, we selected 13 073 galaxies from the NYU-VAGC catalog found in regions on the sky where the feature hosts (that are also in the NYU-VAGC) reside, as shown in Figure 5.1. We recover 601 galaxies with tidal features (58% of the parent sample of feature hosts, Table 5.1) from the NYU-VAGC.

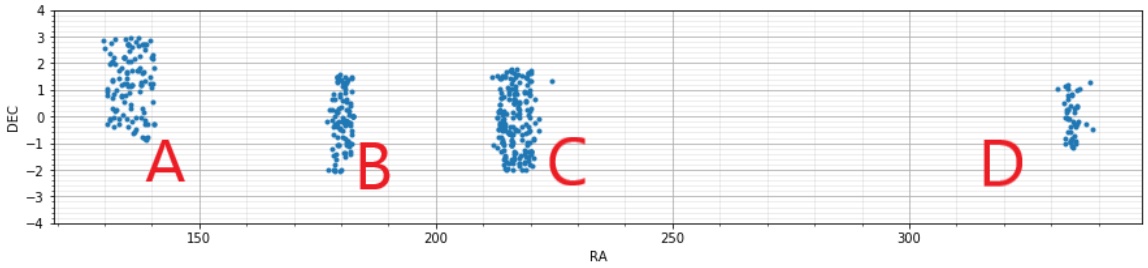

Figure 5.1: Position of stream and shell hosts on the sky. Out of 601 feature hosts found in the NYU-VAGC, 398 have streams and 203 have shells.

5.2 Local Density Measurements for Volume-Limited Samples

5.2.1 Absolute Magnitude Limit

The SDSS sample is flux-limited, that is the observation is biased towards the intrinsically brighter objects with increasing redshift. The number of observed galaxies declines with increasing redshift because the luminosity function, that is the distribution of number density of galaxies with respect to their luminosities, steeply declines at high luminosty (Blanton et al., 2005).

To ensure that our measurement of the local densities are accurate, our galaxy sample need to be completely represented in the survey, without missing observations. To create such a sample, we first find the limiting luminosity as a function of redshift. We find the absolute magnitude M_{abs} from the observed magnitude m_{obs} according to the distance modulus formula:

$$M_{abs} = m_{obs} - 5\log[\frac{D_L}{10pc}] - K, \tag{5.1}$$

where K is the k-correction value available for galaxies from NYU-VAGC, which is used to convert observed magnitude into the rest frame, and D_L is the luminosity distance.

We separate our sample into 20 redshift bins of equal number of galaxies and find the average redshifts, apparent magnitudes and K-correction values within those bins. We then derive the absolute magnitude as a function of redshift by interpolating

between these calculated M_{abs} values based on Equation 5.1.

Figure 5.2 shows the absolute magnitude limit (red line going through orange points) for each region on the sky defined in Figure 5.1. We find that the magnitude limit as a function of redshift is the same in all of the four regions.

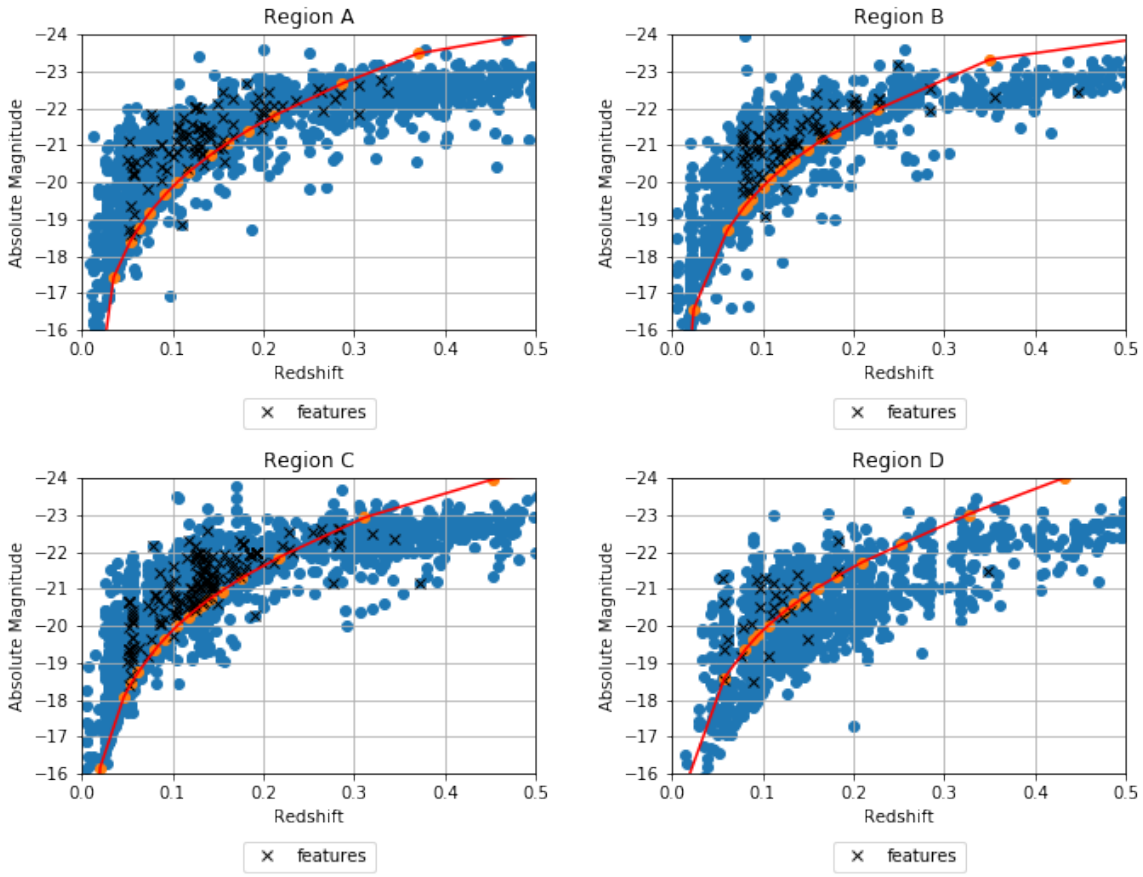

Figure 5.2: Absolute Magnitude versus Redshift diagram showing the flux-limit for each region on the sky defined in Figure 5.1. The blue points shows the selection of 13 073 galaxies from the NYU-VAGC sample and the black crosses shows the position of the feature (shell and stream) hosts in the diagram. The orange points shows the position of the average redshift and absolute magnitude in the 20 redshift bins. The red line shows the absolute magnitude limited function derived from the interpolation of the orange points.

Table 5.2: The table shows the values of redshifts and M_{abs} which outlines the volume-limited samples.

Rectangle	z_{min}	z_{max}	$M_{abs,min}$	$M_{abs,max}$
1	0.00	0.07	-19.0	-24.0
2	0.07	0.11	-20.1	-24.0
3	0.11	0.16	-21.0	-24.0
4	0.16	0.20	-21.6	-24.0

5.2.2 Selecting Volume-Limited Sample

We further separate our sample into volume-limited samples. That is, for galaxies within a given redshift (volume) range and within a given range of absolute magnitudes, which defines a rectangle in the M_{abs}-redshift parameter space (rectangular region bound by yellow lines in Figure 5.3 and detailed in Table 5.2), we have complete observations of their spectra and no correction is needed for unobserved objects (Tempel et al., 2014).

5.2.3 Measurement of Overdensities

For every galaxy in each volume-limited sample selected in the previous section, we use the nearest neighbour approach to determine their environment. We find the distance to the fifth neighbour r_{5NN}, among only galaxies at redshifts that correspond to radial velocities within $\pm$1000 km/s from the target galaxy. We then calculate the surface number density at the redshift of the target galaxy, ρ_{5NN},

$$\rho_{5NN} = \frac{5}{\pi r_{5NN}^2}. \tag{5.2}$$

We represent the overdensity δ as a ratio of ρ_{5NN} to the average surface number

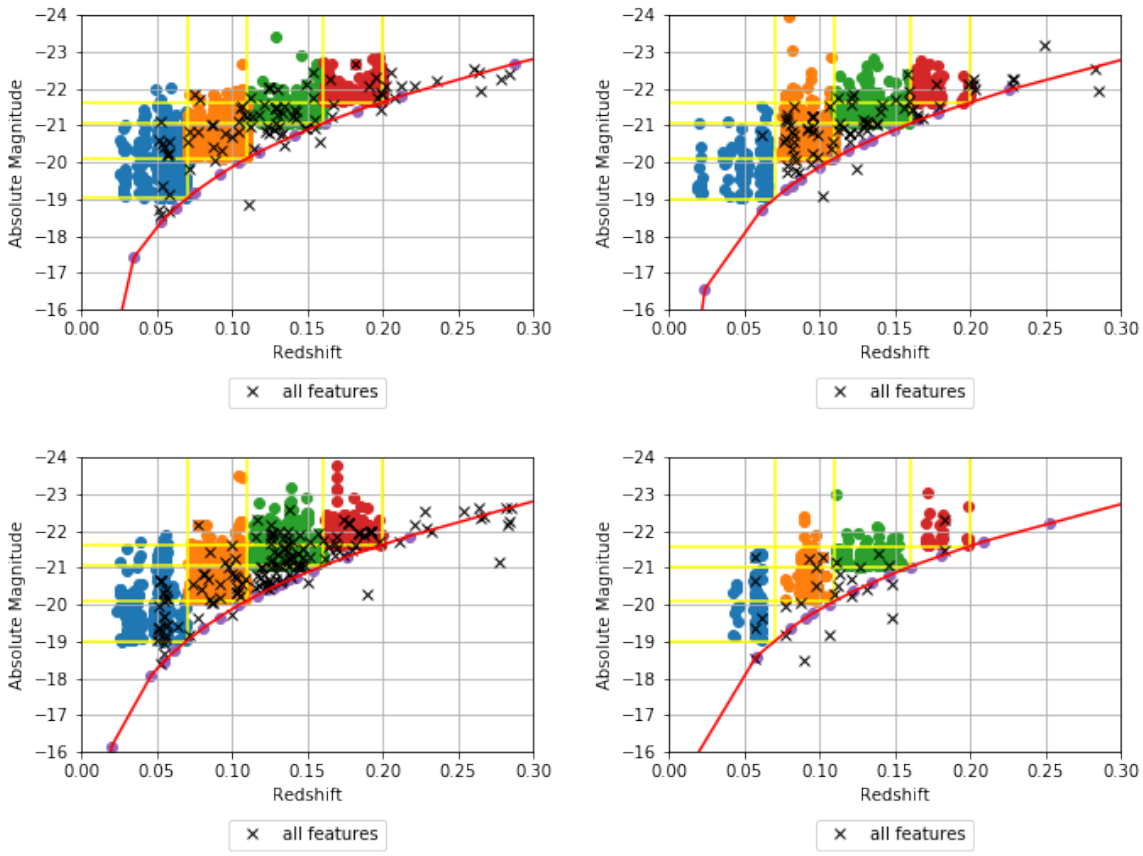

Figure 5.3: The plot is equivalent to Figure 5.2, with yellow lines added showing the outline of the volume-limited sample as described in table 5.2. Galaxies selected in each of these regions are presented with a different colour. We use these galaxies to calculate the local overdensities (Section 5.2.3).

density ρ_{avg} at the redshift of the target galaxy,

$$\delta = \frac{\rho_{5NN}}{\rho_{avg}} - 1 \tag{5.3}$$

The average surface number density ρ_{avg} is

$$\rho_{avg} = \frac{N_z}{A_z} = \frac{N_z}{d_c^2 \frac{\pi^2}{180^2} \Omega} \tag{5.4}$$

where N_z is the total number of objects from the NYU-VAGC at the magnitude

cut and within the radial velocity interval of ±1000 km/s of a given target galaxy, d_c is the comoving distance to the redshift of the target galaxy and Ω is the area of the survey in deg^2 (in our case, 7966 deg^2).

In Figure 5.4 we view the distributions of the overdensities of the galaxies from all four regions on the sky (Figure 5.1) altogether, separated in terms of the redshift slices described in Table 5.2. The population of galaxies from the NYU-VAGC (underlying population) live in overdensities of -1 to 3 and have means around 0.7 at all redshifts. Regions of average local densities would have $\delta = 0$. Thus the general population of galaxies in our NYU-VAGC sample live in slightly overdense environments. We obtain similar results to Weigel et al. (2016), who use the same methods for calculating the overdensity values for a larger subset of the NYU-VAGC sample.

5.3 Local Density Fields around Galaxies that Host Tidal Features

To visualise the distribution of overdensities and the position of galaxies with tidal features with respect to them, we plot the sky position of all NYU-VAGC galaxies with measured local densities (Figure 5.5). We colour-code this distribution of positions by representing the corresponding measured overdensity as the 3^{rd} dimension. Finally, we overplot the sky positions of galaxies harbouring tidal features on top of the distribution of coloured points (i.e. positions of NYU-VAGC galaxies with associated local overdensity measurements). Here in Figure 5.5, we only show galaxies in Region

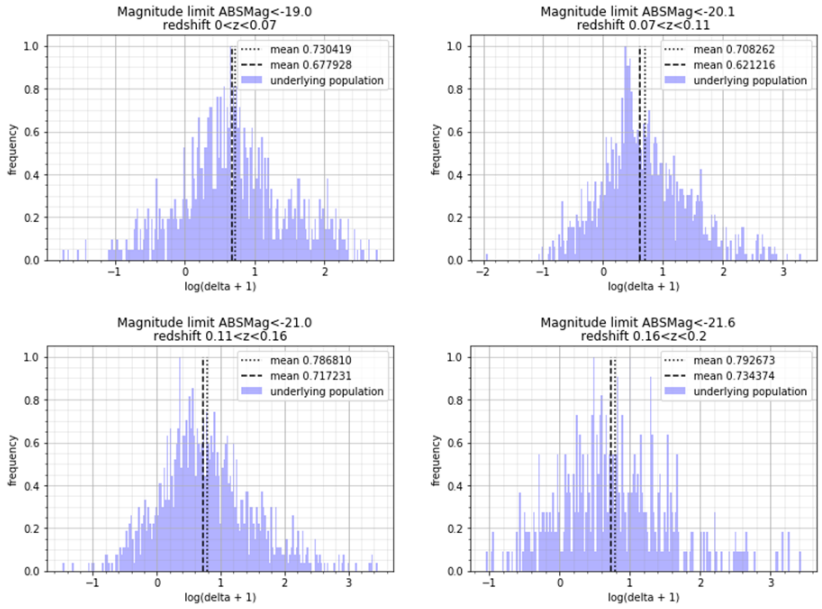

Figure 5.4: Distribution of galaxy overdensities within four redshift bins covered by the NYU-VAGC sample. Plot includes all objects in the four regions A, B, C and D on the sky (Figure 5.1). The 5^{th} and 95^{th} percentiles of the overdensities in all of the redshift bins are at -0.6 to 2 and have means around 0.7, thus the average overdensities at all redshift bins are in slightly overdense regions ($\delta > 0$).

C (defined in Figure 5.1), since the region contains the more feature hosts (shells and stream) than the other regions, and thus provide a better representation of our observations (overdensity maps for regions A, B, and D are shown in Appendix A). Each panel in the figure shows different redshift slices (described in Table 5.2). With increasing redshift, due to the limitations of the survey, we are only able to probe brighter and brighter galaxies.

To obtain a smooth distribution of overdensities and under densities in the plane of the sky, we use a Python implementation of the Locally Weighted Scatterplot Smoothing (LOESS) method, developed by Cleveland and Devlin (1988, Figure 5.6). From visual inspection of the Figures 5.5 and 5.6, we can conclude that, on average,

galaxies with tidal features tend to avoid the most extreme overdensity regions (cluster cores) as well as regions with extreme underdensities (voids).

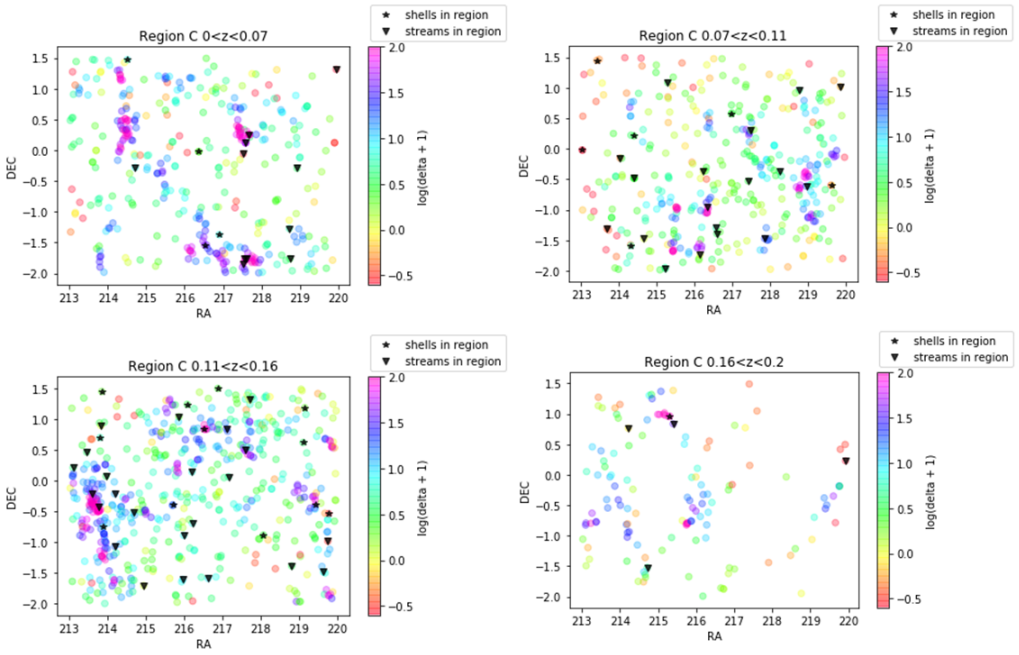

Figure 5.5: Map of the sky of Region C (defined in Figure 5.1) showing positions of NYU-VAGC galaxies colour-coded according to their overdensities. Overplotted black triangles and stars represent positions of stream and shell hosts. Each panel shows a redshift slice defined in Table 5.2.

To quantify qualitative results based on the previous two figures, we determine the overdensities of galaxies with tidal features and compare them to the underlying general population of NYU-VAGC galaxies. We find the local density corresponding to a feature host by associating the overdensity δ of its nearest neighbour from NYU-VAGC galaxies, within a radial velocity of $\pm$1000 km/s to the target host galaxy.

We compare the cumulative distributions of the overdensitites of the underlying population (galaxies in NYU-VAGC) to that of the galaxies with tidal features in different magnitude and redshift slices defined in Figure 5.3. Our results (Figure 5.7) show that feature hosts do not live in the highest density regions measured (clusters)

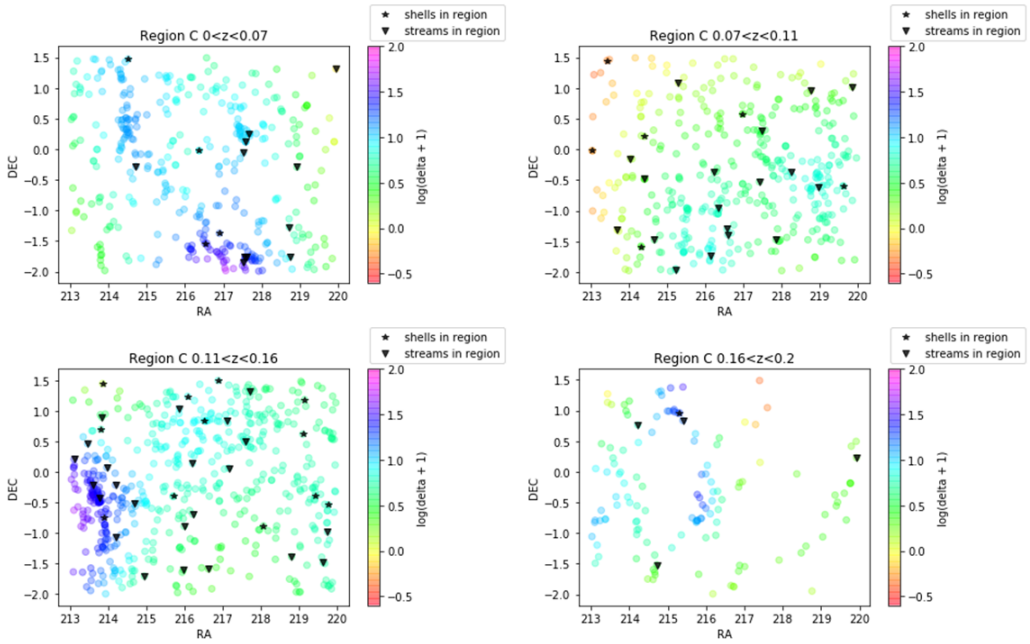

Figure 5.6: Figure is equivalent to Figure 5.5 except that the colour-coding of the NYU-VAGC galaxies is now representing a smooth distribution of over-densities, derived from the LOESS method. Feature hosts tend to be found in intermediate density regions, with colours which span from green to blue.

and that at low and intermediate redshifts ($0 < z < 0.07$ and $0.11 < z < 0.16$) there is a tail of streams at low density regions.

In the bottom left panel of Figure 5.7 for galaxies at redshift $0.11 < z < 016$, the results from the Anderson-Darling test[1] (AD test, Stephens, 1974) show that the null hypotheses that the samples of stream and shell hosts and that of the underlying general population come from the same distribution can be rejected at 6% and 8%, respectively. This resulting significance is large enough for us to conclude that the two distributions are not sampled from the same population.

We also perform a similar analysis to the one described in Section 4.2 for galaxies in the redshift cuts $0.07 < z < 0.11$ and $0.11 < z < 0.16$, where we sample galaxies

[1]The AD test is analogous to the KS test, but is more sensitive to the tail of the distribution

from the parent sample with stellar mass distribution matching that of the galaxies hosting streams or shells (Figure 5.8). These results show that galaxies with shells live in slightly higher density regions than galaxies in NYU-VAGC with similar stellar mass distribution.Furthermore, shell hosts lie in rather higher overdensity regions ($\delta > 2.0$) than stream hosts (based on the comparison of the extent of x-axes in the left and right column of Figure 5.8). Redder and more massive galaxies have been shown to live in denser regions (Muldrew et al., 2012). We find that shell hosts have higher stellar mass (Section 3.1) and they tend to be redder (Kado-Fong et al., 2018), thus it is expected that they are in regions with higher overdensities.

The tidal feature hosts are more abundant in the intermediate density regions (overdensities between 0 and 2), thus they are not completely isolated, nor do they belong to clusters. It is expected that they live in galaxy groups where the velocity dispersion is not as strong as in galaxy clusters, thus allowing mergers (Ravel et al., 2011).

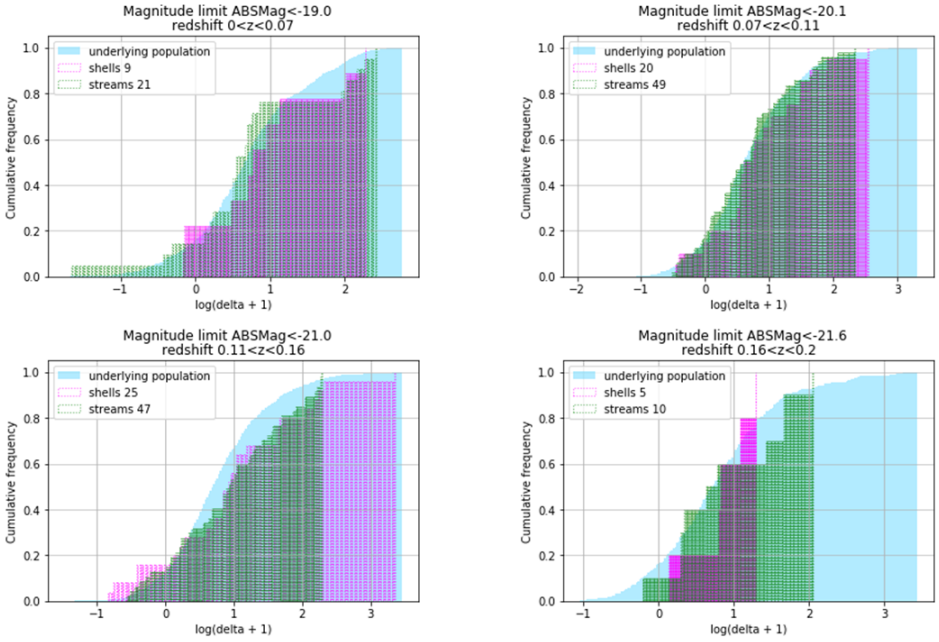

Figure 5.7: Cumulative frequency distribution of overdensities comparing parent sample and feature hosts at each redshift bin. Tidal feature hosts do not live in the highest overdensities at all redshifts. Tail of streams seen at low overdensities at redshifts $0.0 < z < 0.07$ and $0.11 < z < 0.16$.

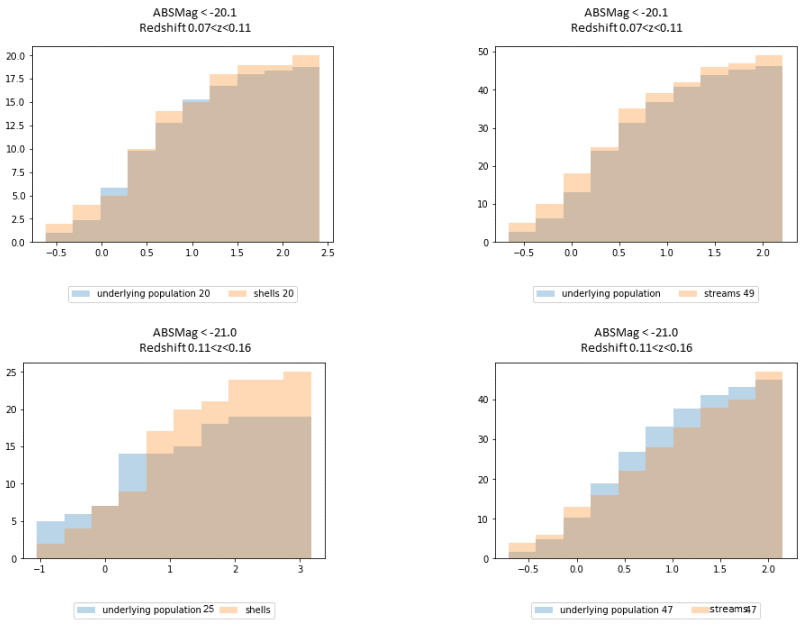

Figure 5.8: Figure shows the cumulative distribution of the overdensities of galaxies with shells (right) and streams (left), compared to NYU-VAGC galaxies of similar stellar masses. Top rows shows galaxies in redshift slice $0.07 < z < 0.11$ and the bottom row shows those in $0.11 < z < 0.16$. Shell hosts tend to be in denser regions than both stream hosts and the general population of galaxies.

Chapter 6

Conclusion and Future Works

We use the galaxy sample at redshifts $0.05 < z < 0.45$ from Kado-Fong et al. (2018), with their associated spectroscopic measurements from SDSS catalogs, to study the properties of galaxies with tidal features. We reclassify the whole sample of 21208 galaxies visually and detected 251 shells and 774 streams. We analyse the internal properties of galaxies with tidal features and compare them to the general population of galaxies of similar mass. We derive star formation rates and BPT classifications from available emission line measurements. We use redshifts and magnitudes from the NYU-VAGC to determine the local densities of the galaxies surrounding systems harbouring streams and shells.

Our main findings are:

- Shell hosts are more massive than galaxies with streams and the general population of galaxies. This is consistent with theoretical predictions (Pop et al., 2017) that shells are the results of major mergers which cause a significant increase in the stellar mass of the resulting merger remnant.

- Galaxies with shells are older than both featureless galaxies and stream hosts. This paints the picture in which shells are formed later in the galaxy merger history and that their presence lingers on much after the merger happened.

- The distributions for stellar mass and age of galaxies harbouring streams span the full range of measurements of mass and age of the general population of galaxies. This suggests that streams can occur in galaxies at different stages of their evolution.

- Stream hosts are on average slightly younger than the general population of galaxies. The explanation for this trend may be that streams are formed earlier on in the galaxy's merger history and may diffuse or evolve into shell as the galaxy ages(Cooper et al., 2011).

- Galaxies with shells have low star formation rates (they are mainly found in the quiescent region of the distribution of the general population of galaxies). This relates to the previous observations that shell hosts are older and more massive. The quenching of these galaxies may also be caused by a process related to the formation of shells.

- Galaxies with streams, on the other hand, have star formation rates spread over the full range of measurements. Even massive stream hosts have high rates of star formation. We speculate is that streams can funnel enough gaseous material into their hosts to boost star formation.

- Emission line galaxies with shells are more likely to be among composite galaxies and LINERs in the BPT diagram. These galaxies show the presence of AGN activity and low star formation rates. This may indicate that a combination of star formation feedback and low-level AGN activity may play a role in the

formation of some shells.

- In comparison to the general population matched in mass, a larger fraction of stream hosts wit emission lines are Seyferts. We stipulate that streams may be fueling material into the central region of the galaxy, growing the accretion disk.

- Tidal feature hosts do not live in the highest overdensity regions (cluster cores), nor in the lowest density regions (isolated). This is consistent with the fact that clusters suppresses mergers and that galaxies require slightly overdense regions (e.g. groups) for merging to happen.

- Stream hosts can be found at some redshifts in regions of low densities (isolated). They may be deprived of neighbours of significant masses, but may have small satellites allowing minor mergers that produce streams.

- Shell hosts tend to be in slightly higher density regions than the general population of galaxies of similar mass. Shell hosts are in general redder and more massive, which is in agreement with our finding that they live in denser region.

- Feature hosts, regardless of whether or not they have shells or streams, on average live in the same environments (intermediate regions). This may relate to the idea that streams evolve into shells as the resulting galaxy ages after merging (Cooper et al., 2011). However this may be only happening for certain types of galaxies where the internal properties are suitable (interaction between high mass galaxies, result of major mergers).

Our sample of streams and shells clearly provides seeds for future work. This sample can be further extended by developing effective machine learning approaches for the detection and classification of tidal features in large survey.

Some possible subsequent studies are:

- Examining the metallicity and composition of specific stream hosts to confirm that the gaseous materials in the streams is connected with the star forming regions of the hosts.

- Studying tidal feature hosts in the X-ray regime can give a better insight of the relationship between the tidal features and the presence of AGN.

- Determining the local density of host galaxies using photometry would allow us to probe fainter neighbours around the feature hosts, which will tell us more about minor interactions between the galaxies.

Appendix A

Overdensity Maps

We present the overdensities described in Section 5.2.3 for Regions A, B and D of Figure 5.1. Here we show Figures A.1, A.2, A.3, A.4, A.5 and A.6 , for the maps of the local density of the underlying population of galaxies and the accompanying tidal feature hosts.

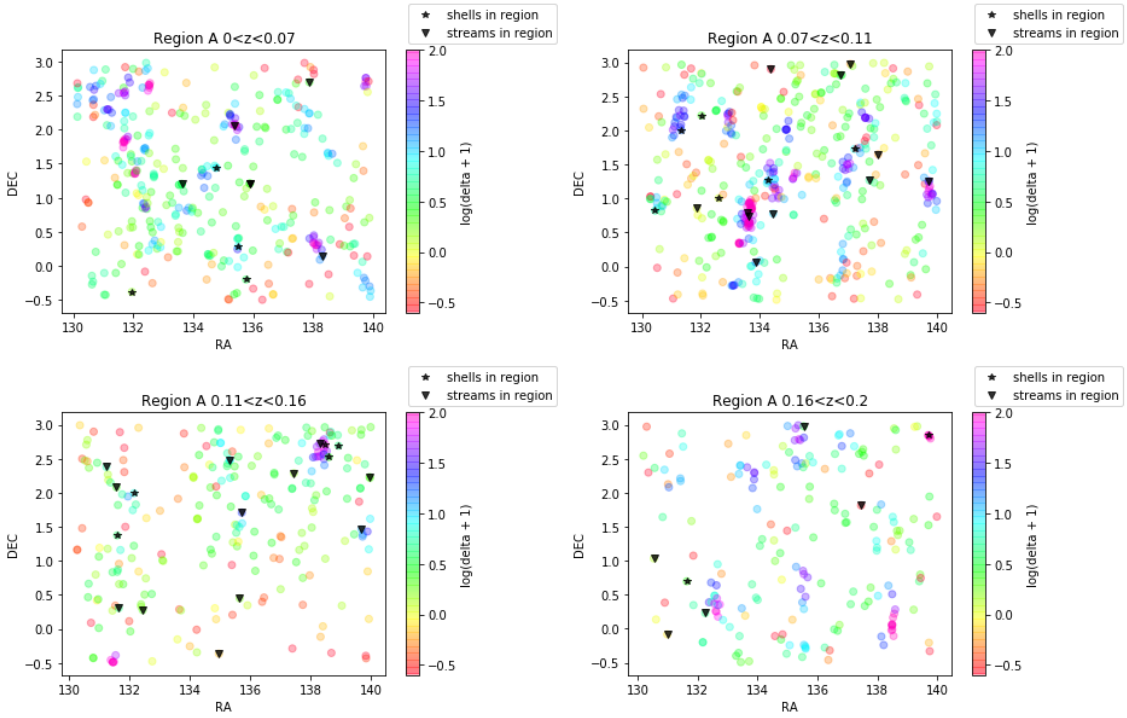

Figure A.1: Map of the sky of Region A (defined in Figure 5.1) showing positions of NYU-VAGC galaxies colour-coded according to their overdensities. Overplotted black triangles and stars represent positions of stream and shell hosts. Each panel shows a redshift slice defined in Table 5.2.

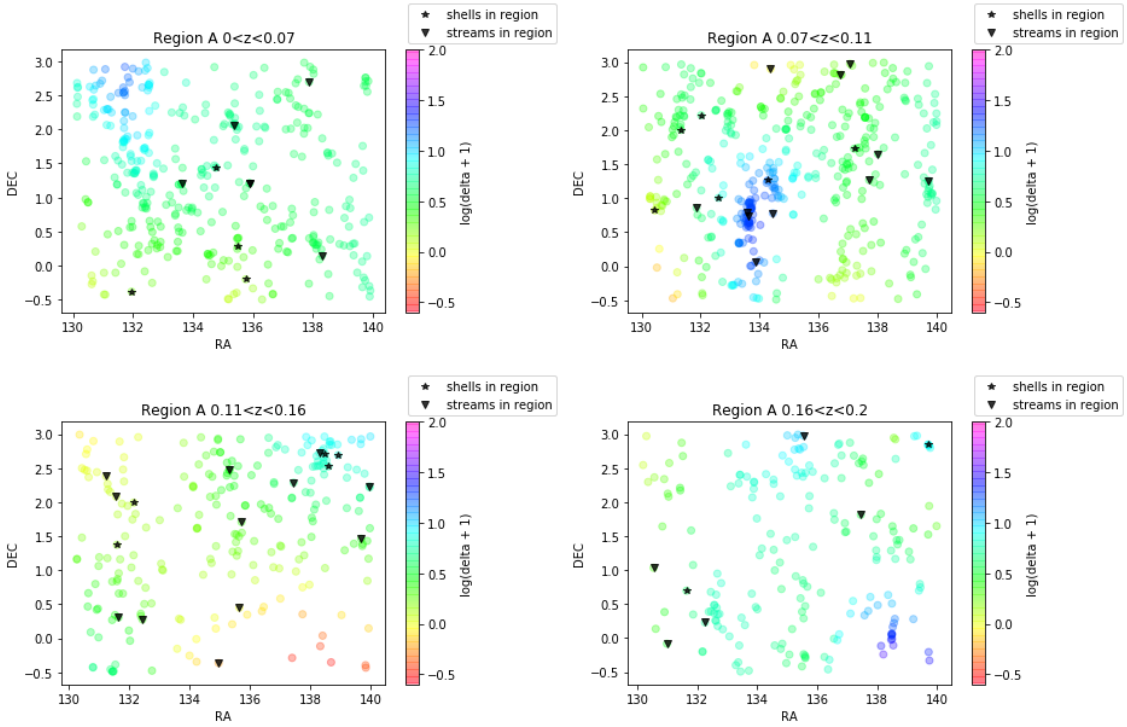

Figure A.2: Figure is equivalent to Figure A.1 except that the colour-coding of the NYU-VAGC galaxies is now representing a smooth distribution of overdensities, derived from the LOESS method. Feature hosts tend to be found in intermediate density regions, with colours which span from green to blue.

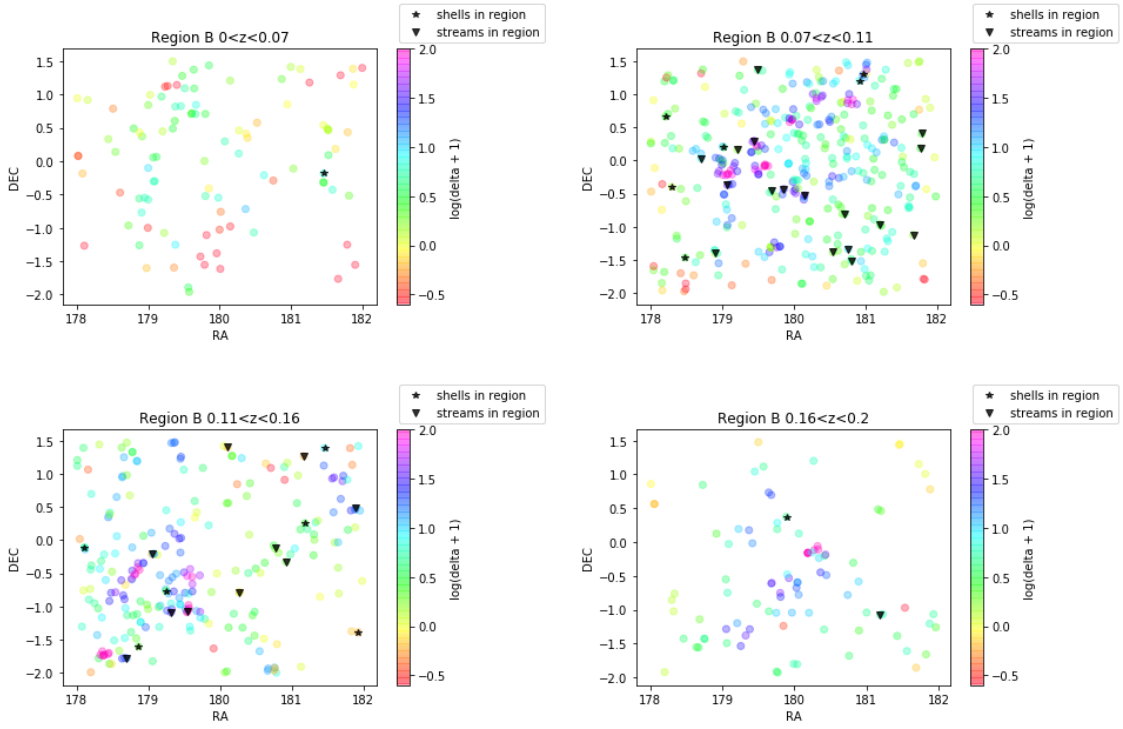

Figure A.3: Map of the sky of Region B (defined in Figure 5.1) showing positions of NYU-VAGC galaxies colour-coded according to their overdensities. Overplotted black triangles and stars represent positions of stream and shell hosts. Each panel shows a redshift slice defined in Table 5.2.

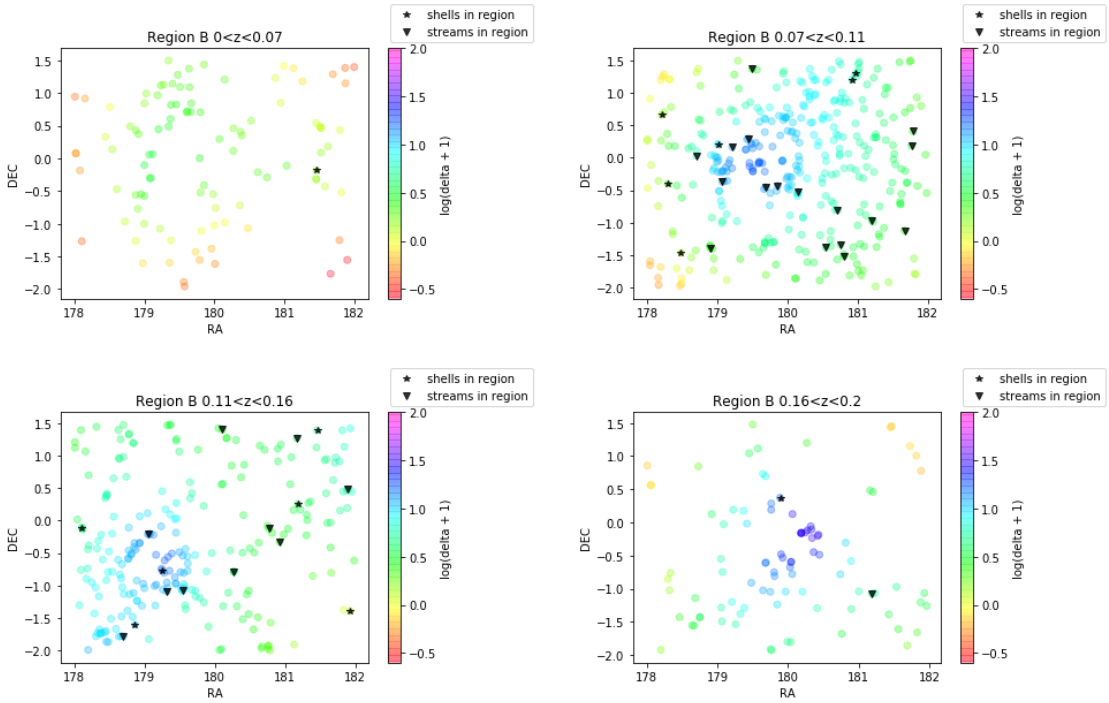

Figure A.4: Figure is equivalent to Figure A.3 except that the colour-coding of the NYU-VAGC galaxies is now representing a smooth distribution of overdensities, derived from the LOESS method. Feature hosts tend to be found in intermediate density regions, with colours which span from green to blue.

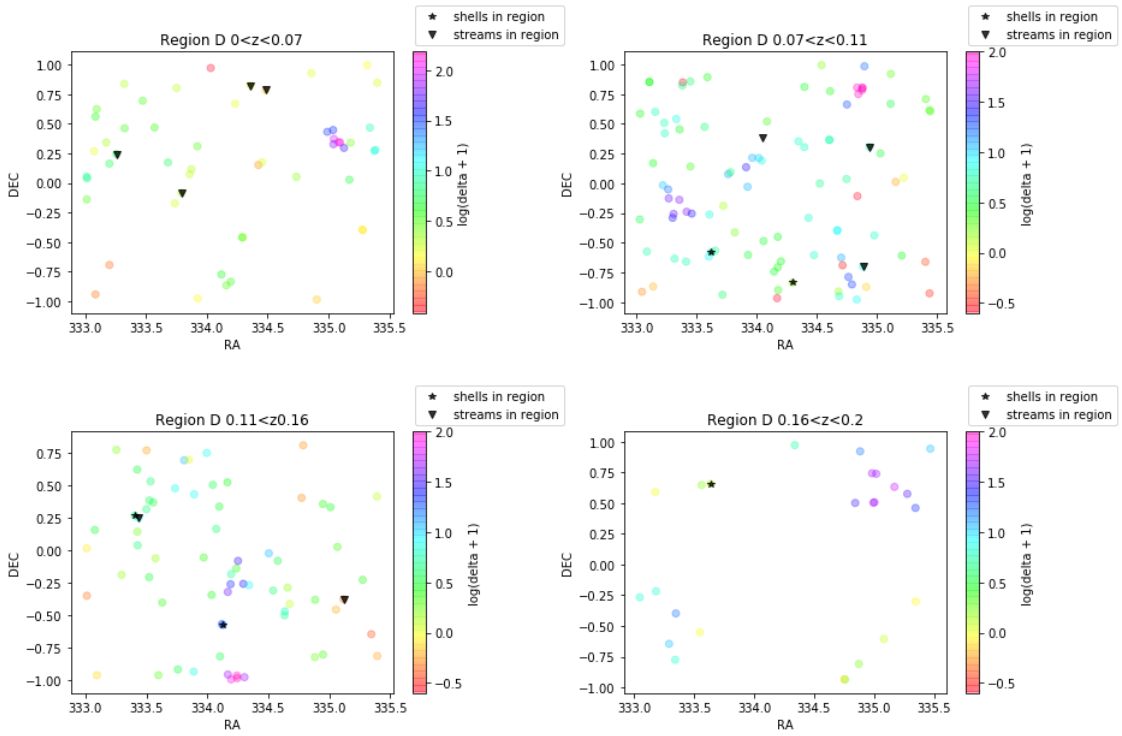

Figure A.5: Map of the sky of Region D (defined in Figure 5.1) showing positions of NYU-VAGC galaxies colour-coded according to their overdensities. Overplotted black triangles and stars represent positions of stream and shell hosts. Each panel shows a redshift slice defined in Table 5.2.

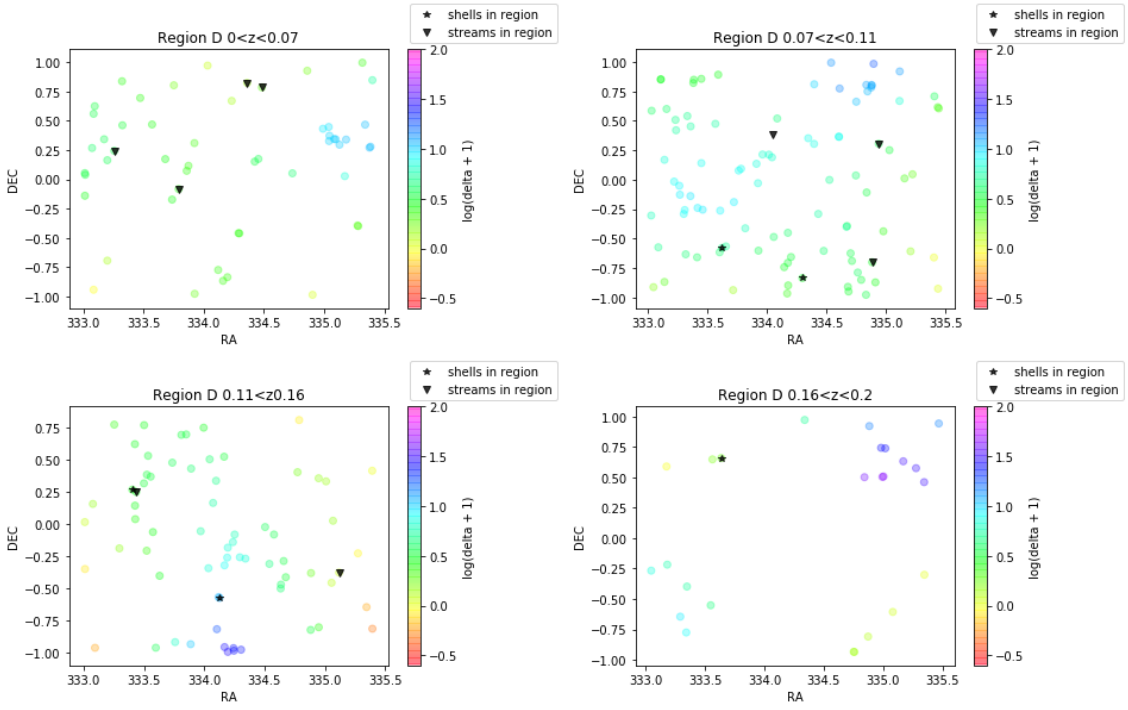

Figure A.6: Figure is equivalent to Figure A.5 except that the colour-coding of the NYU-VAGC galaxies is now representing a smooth distribution of overdensities, derived from the LOESS method. Feature hosts tend to be found in intermediate density regions, with colours which span from green to blue.

Bibliography

Hiroaki Aihara et al. The Hyper Suprime-Cam SSP Survey: Overview and survey design. *Publications of the Astronomical Society of Japan*, 70:S4, January 2018.

Shadab Alam et al. The eleventh and twelfth data releases of the sloan digital sky survey: Final data from sdss-iii. *The Astrophysical Journal Supplement Series*, 219 (1):12, Jul 2015.

J. A. Baldwin et al. Classification parameters for the emission-line spectra of extragalactic objects. *Publication of the Astronomical Society of the Pacific*, 93:5–19, February 1981.

Michael R. Blanton et al. New York University Value-Added Galaxy Catalog: A Galaxy Catalog Based on New Public Surveys. *Astronomical Journal*, 129(6):2562–2578, June 2005.

J. Brinchmann, Charlot, et al. The physical properties of star-forming galaxies in the low-redshift Universe. *Monthly Notices of the Royal Astronomical Society*, 351 (4):1151–1179, July 2004.

G. Bruzual A. Spectral evolution of galaxies. I. Early-type systems. *The Astrophysical Journal*, 273:105–127, October 1983.

William S. Cleveland and Susan J. Devlin. Locally weighted regression: An approach to regression analysis by local fitting. *Journal of the American Statistical Association*, 83(403):596–610, 1988.

Charlie Conroy. Modeling the Panchromatic Spectral Energy Distributions of Galaxies. *Annual Reviews of Astronomy and Astrophysics*, 51(1):393–455, August 2013.

Andrew P. Cooper et al. The formation of shell galaxies similar to ngc 7600 in the cold dark matter cosmogony. *The Astrophysical Journal*, 743(1):L21, Nov 2011.

E. Daddi et al. Multiwavelength study of massive galaxies atz∼2. i. star formation and galaxy growth. *The Astrophysical Journal*, 670(1):156–172, nov 2007.

Kyle S. Dawson et al. Spectroscopic Target Selection in the Sloan Digital Sky Survey: The Main Galaxy Sample. *Astronomical Journal*, 124(3):1810–1824, September 2002.

Elbaz et al. The reversal of the star formation-density relation in the distant universe. *Astronomy and Astrophysics*, 468(1):33–48, June 2007.

Sara L. Ellison et al. The mass-metallicity relation in galaxy clusters: the relative importance of cluster membership versus local environment. *Monthly Notices of the Royal Astronomical Society*, 396(3):1257–1272, July 2009.

A. C. Fabian et al. Star formation in a galactic wind. *Nature*, 287(5783):613–614, October 1980.

N. Gehrels. Confidence Limits for Small Numbers of Events in Astrophysical Data. *Astrophysical Journal*, 303:336, April 1986.

David Hendel et al. Tidal debris morphology and the orbits of satellite galaxies. *Monthly Notices of the Royal Astronomical Society*, 454(3):2472–2485, December 2015.

Kathryn V. Johnston et al. Interpreting Debris from Satellite Disruption in External Galaxies. *The Astrophysical Journal*, 557(1):137–149, August 2001.

Kado-Fong et al. Tidal Features at $0.05 < z < 0.45$ in the Hyper Suprime-Cam Subaru Strategic Program: Properties and Formation Channels. *The Astrophysical Journal*, 866(2):103, October 2018.

Kang et al. The role of environment on the star formation history of disc galaxies. *Monthly Notices of the Royal Astronomical Society*, 469(2):1636–1646, August 2017.

Marvin Karson. Handbook of methods of applied statistics. volume i: Techniques of computation descriptive methods, and statistical inference. volume ii: Planning of surveys and experiments. *Journal of the American Statistical Association*, 63(323): 1047–1049, 1968.

Guinevere Kauffmann et al. Stellar masses and star formation histories for 10^5 galaxies from the Sloan Digital Sky Survey. *Monthly Notices of the Royal Astronomical Society*, 341(1):33–53, May 2003.

Kennicutt. Star Formation in Galaxies Along the Hubble Sequence. *Annual Review of Astronomy and Astrophysics*, 36:189–232, January 1998.

L. J. Kewley et al. Optical Classification of Southern Warm Infrared Galaxies. *Astrophysical Journal Supplement Series*, 132(1):37–71, January 2001.

Lisa J. Kewley et al. The host galaxies and classification of active galactic nuclei. *Monthly Notices of the Royal Astronomical Society*, 372(3):961–976, November 2006.

X. Kong et al. Spectroscopic study of blue compact galaxies. II. Spectral analysis and correlations. *Astronomy and Astrophysics*, 396:503–512, December 2002.

Giovanni La Mura et al. Models of Emission-Line Profiles and Spectral Energy Distributions to Characterize the Multi-Frequency Properties of Active Galactic Nuclei. *Atoms*, 5(4):43, November 2017.

Claudia Maraston et al. Modelling the colour evolution of luminous red galaxies - improvements with empirical stellar spectra. *Monthly Notices of the Royal Astronomical Society*, 394(1):L107–L111, March 2009.

Claudia Maraston et al. Stellar population models at high spectral resolution. *Monthly Notices of the Royal Astronomical Society*, 418(4):2785–2811, dec 2011.

Stuart I. Muldrew et al. Measures of galaxy environment - I. What is 'environment'? *Monthly Notices of the Royal Astronomical Society*, 419(3):2670–2682, January 2012.

K. G. Noeske et al. Star formation in AEGIS field galaxies since z =1.1: The dominance of gradually declining star formation, and the main sequence of star-forming galaxies. *The Astrophysical Journal*, 660(1):L43–L46, apr 2007.

Ana-Roxana Pop et al. Galaxies with Shells in the Illustris Simulation: Metallicity Signatures. *Galaxies*, 5(3):34, August 2017.

L. Ravel et al. The zcosmos redshift survey : Influence of luminosity, mass and environment on the galaxy merger rate. *Astronomy Astrophysics*, 2011.

Peter Schneider. *The world of galaxies. In: Extragalactic Astronomy and Cosmology.* Springer, Berlin, Heidelberg, 2015.

Linda S. Sparke et al. *Galaxies in the Universe: An Introduction.* 2007.

M. A. Stephens. Edf statistics for goodness of fit and some comparisons. *Journal of the American Statistical Association*, 69(347):730–737, 1974.

Michael A. Strauss et al. Spectroscopic Target Selection in the Sloan Digital Sky Survey: The Main Galaxy Sample. *Astronomical Journal*, 124(3):1810–1824, September 2002.

E. Tempel et al. Flux- and volume-limited groups/clusters for the SDSS galaxies: catalogues and mass estimation. *Astronomy and Astrophysics*, 566:A1, June 2014.

Daniel Thomas et al. Flux-calibrated stellar population models of Lick absorption-line indices with variable element abundance ratios. *Monthly Notices of the Royal Astronomical Society*, 412(4):2183–2198, apr 2011.

Jeremy L. Tinker and Charlie Conroy. The Void Phenomenon Explained. *Astrophysical Journal*, 691(1):633–639, January 2009.

M. P. Véron-Cetty et al. The emission line spectrum of active galactic nuclei and the unifying scheme. *Astronomy and Astrophysics Review*, 10:81–133, January 2000.

M. Vitale et al. Investigating the relationship between AGN activity and stellar mass in zCOSMOS galaxies at $0 < z < 1$ using emission-line diagnostic diagrams. *Astronomy and Astrophysics*, 556:A11, August 2013.

Anna K. Weigel, Kevin Schawinski, and Claudio Bruderer. Stellar mass functions: methods, systematics and results for the local Universe. *Monthly Notices of the Royal Astronomical Society*, 459(2):2150–2187, 04 2016.

Katherine E. Whitaker et al. Predicting Quiescence: The Dependence of Specific Star Formation Rate on Galaxy Size and Central Density at $0.5 < z < 2.5$. *The Astrophysical Journal*, 838(1):19, March 2017.

R. E. Williams and W. A. Christiansen. Blast wave formation of the extended stellar shells surrounding elliptical galaxies. *Astrophysical Journal*, 291:80–87, April 1985.

Stijn Wuyts et al. Galaxy Structure and Mode of Star Formation in the SFR-Mass Plane from z ~2.5 to z ~0.1. *Astrophysical Journal*, 742(2):96, December 2011.

Kastytis Zubovas et al. Do AGN outflows quench or enhance star formation? *Monthly Notices of the Royal Astronomical Society*, 468(4):4956–4967, 03 2017.